ASTRONOMY & ASTROPHYSICS
SUPPLEMENT SERIES

Astron. Astrophys. Suppl. Ser. **142**, 275–311 (2000)

The Vienna-KPNO search for Doppler-imaging candidate stars

I. A catalog of stellar-activity indicators for 1058 late-type Hipparcos stars⋆

K.G. Strassmeier⋆⋆, A. Washuettl⋆⋆, Th. Granzer⋆⋆, M. Scheck, and M. Weber⋆⋆

Institut für Astronomie, Universität Wien, Türkenschanzstraße 17, A-1180 Wien, Austria
e-mail: name@astro.univie.ac.at

Received November 2; accepted December 22, 1999

Abstract. We present the results from a spectroscopic Ca II H&K survey of 1058 late-type stars selected from a color-limited subsample of the *Hipparcos* catalog. Out of these 1058 stars, 371 stars were found to show significant H&K emission, most of them previously unknown; 23% with strong emission, 36% with moderate emission, and 41% with weak emission. These spectra are used to determine absolute H&K emission-line fluxes, radial velocities, and equivalent widths of the luminosity-sensitive Sr II line at 4077 Å. Red-wavelength spectroscopic and Strömgren y photometric follow-up observations of the 371 stars with H&K emission are used to additionally determine the absolute Hα-core flux, the lithium abundance from the Li I 6708 Å equivalent width, the rotational velocity $v \sin i$, the radial velocity, and the light variations and its periodicity. The latter is interpreted as the stellar rotation period due to an inhomogeneous surface brightness distribution. 156 stars were found with photometric periods between 0.29 and 64 days, 11 additional systems showed quasi-periodic variations possibly in excess of ≈50 days. Further 54 stars had variations but no unique period was found, and four stars were essentially constant. Altogether, 170 new variable stars were discovered. Additionally, we found 17 new SB1 (plus 16 new candidates) and 19 new SB2 systems, as well as one definite and two possible new SB3 systems. Finally, we present a list of 21 stars that we think are most suitable candidates for a detailed study with the Doppler-imaging technique.

Key words: stars: activity — stars: chromospheres — stars: late-type — stars: rotation — surveys

⋆ Tables A1–A3 are only available in electronic form at the CDS via anonymous ftp to cdsarc.u-strasbg.fr (130.79.128.5) or via http://cdsweb.u-strasbg.fr/Abstract.html

⋆⋆ Visiting Astronomer, Kitt Peak National Observatory, operated by the Association of Universities for Research in Astronomy, Inc. under contract with the National Science Foundation.

1. Scientific motivation for a Ca II H&K survey

The presence of emission in the core of the Ca II H and K resonance lines is a diagnostic of magnetic activity in the chromospheres of late-type stars. Spatially resolved K-line heliograms and magnetograms amply demonstrate the relation between H&K-emission strength and the surface magnetic field on our Sun (Schrijver 1996). Furthermore, the fact that we observe generally stronger H&K emission in more rapidly rotating stars is widely known as the rotation-activity relation (e.g. Noyes et al. 1984) which is heuristically explained by the Ω-effect of the classic $\alpha\Omega$ dynamo (see Stix 1989). Therefore, rapidly-rotating stars offer laboratories to study the effect of stellar dynamos. The catalog of chromospherically active binary stars (CABS, Strassmeier et al. 1993) summarized such stars in binaries and proofed to be a valuable data base for further investigations.

It is only the very rapidly-rotating stars where we can also obtain spatially resolved information of their surface temperature distribution, and respectively also of their magnetic surface field, by applying indirect imaging techniques like Doppler imaging (e.g. Rice 1996). Such rapidly-rotating active stars are relatively rare but can be identified from their Ca II H&K emission with just a single spectrum of low signal-to-noise ratio and moderate resolution. For example, a H&K survey from low-resolution spectra in the southern hemisphere (Henry et al. 1996) provided the source for the discovery of many rapidly-rotating solar-type stars (Soderblom et al. 1998). The H&K work of W. Bidelman (e.g. Bidelman 1981; see also Sect. 2) supplied the target lists for the radial-velocity and photometric survey at SAAO (e.g. Balona 1987; Lloyd-Evans & Koen 1987).

Another particularly important example of an usolved question in the above context is the angular momentum loss during stellar evolution. Magnetic braking of stellar rotation due to a stellar wind along predominantly equatorial magnetic field lines, like in our Sun, seemed not to have always the power to

slow down stars from their initial angular momentum gained during the contraction from the pre-stellar cloud. The many ultra-fast rotators in young open clusters as well as the young field stars AB Dor, LQ Hya, EK Dra etc. are the most cited examples. Moreover, there exists a group of single, rapidly-rotating and *evolved* stars with strong magnetic activity (Fekel & Balachandran 1993). This is a paradox since magnetic braking had enough time during the main-sequence stage to halt the rapid rotation, and the radius increase due to the termination of hydrogen-core burning should have resulted in an effectively complete loss of angular momentum. What process maintained these stars angular momentum? Is it the same process suggested for the ultra-rapid cluster rotators, i.e. a saturation of the atmospheric (coronal) volume with magnetic fields so that there is no torque arm for magnetic braking via a stellar wind anymore? Or is it something completely different?

Solanki et al. (1997), Strassmeier et al. (1998) and Buzasi (1999) suggested that magnetic fields concentrated in polar starspots could be the reason for such a lack of angular-momentum loss as described above. Solanki et al. presented numerical simulations that show that the effect would be quantitatively the same as with a dynamo saturation process. The only way to find conclusive observational evidence for or against the polar-spot hypothesis is to Doppler image these stars and search for polar starspots. Since Doppler imaging is an elaborate technique with many restrictions for the stellar sample (rapid rotation, medium inclination, known rotation period, relatively bright star etc.) one needs significantly more stellar candidates as known to date to cover the part in the $\mathrm{H-R}$ diagram where stellar activity occurs. It is the primary aim of this survey to provide a larger sample of suitable Doppler-imaging targets. Additional goals are to provide activity-related stellar parameters like absolute Ca II emission-line fluxes, the Hα morphology, the lithium abundance, and photometric variations and relate them to absolute stellar parameters based on the distance from the *Hipparcos* satellite.

2. Goals and observing procedure

We have selected a subsample of late-type stars from the ESA *Hipparcos* catalog (ESA 1997) in the brightness range $7\overset{\mathrm{m}}{.}0 - 9\overset{\mathrm{m}}{.}5$ and declination $-30°$ through +70°. $B-V$ colors between 0.67 and 1.0 for stars with parallaxes $\pi > 20$ milli-arcsec (i.e. G5–K3 dwarfs) and between 0.87 and 1.2 for $3 < \pi < 20$ milli-arcsec (i.e. G5–K2 giants and subgiants) select the range of stars with convective envelopes and thus likely magnetic activity. Out of this sample of 6440 stars, 460 were observed in September 1998 in the right-ascension range 18^{h}–6^{h}, and 598 in February 1999 in the right-ascension range 6^{h}–18^{h}. Generelly, we excluded stars that already had a published moderate-to-high resolution Ca II spectrum but in some interesting cases we reobserved them. Previously known H&K emission-line stars came mostly from the following sources: the original Wilson sample of photographic-plate spectra (e.g. Wilson 1976), the spectrophotometric Mt. Wilson H&K survey (e.g. Duncan et al. 1991), Bidelman's catalogue and bibliography of emission-line stars of types later than B (Bidelman 1954), the Michigan-University southern and northern sky objective-prism survey (Bidelman & MacConnell 1973; Bidelman 1981, 1983, 1985, 1988), the lists of Fekel and collaborators (e.g. Fekel et al. 1986), the CDS data base collected by Lastennet & Freire Ferrero (1994), and our own Ca II data of active stars (Strassmeier et al. 1990, 1993; Strassmeier 1994).

Our observing procedure was as follows. After H&K emission was detected from a short-exposure spectrum centered near 4000 Å, we reobserved the star at red wavelengths. These spectra include the Hα line and the lithium line at 6707 Å and are used to determine their respective line properties and a more precise value for the rotational broadening as is possible from the blue spectra. The additional radial velocity from the red spectrum may also indicate whether the star is an unknown spectroscopic binary. It is also of higher precision due to lesser line blending in the red. If the star had H&K emission, we added it to the observing menu of one of our two automatic photoelectric telescopes (APTs) in southern Arizona. These data are used to search for light variations and to determine a photometric period that is then assumed to be the stellar rotation period.

Figure 1 shows the sky coverage and galactic distribution of all target stars observed. Large dots denote the stars that were found to exhibit H&K emission, small dots those without emission. Figure 2 plots the distribution of stellar parameters within the entire sample. V magnitudes and $B-V$ colors were taken from the Tycho catalog and trigonometric parallaxes from the Hipparcos catalog (ESA 1997). The effective temperatures are based on the $B-V$ calibration from Flower (1996). Table A1 lists the stars with H&K emission, Table A2 those without emission. Both tables are available only in electronic form.

3. Observations

3.1. Spectroscopy

All spectroscopic observations in this paper were obtained with the 0.9-m coudé feed telescope at Kitt Peak National Observatory (KPNO) during runs in September 10–23, 1998 and February 11 through March 3, 1999 (a few spectra were added from an earlier run in April 1998). Data were obtained with a 3000×1000 CCD (Ford F3KB chip, 15μ pixels) with grating A, camera 5, the blue corrector, and the long collimator. Spectra were obtained at blue wavelengths centered at 4020 Å to cover the two Ca II H&K resonance lines at 3933 Å and 3968 Å as well as the luminosity-sensitive strontium line, Sr II, at 4077 Å. Stars with Ca II emission were also observed at red wavelengths centered at 6630 Å to cover the Balmer Hα line at 6563 Å and the neutral lithium line at 6708 Å. The useful wavelength coverage was 210 Å in the blue region and 300 Å in the red wavelength region. The resolving

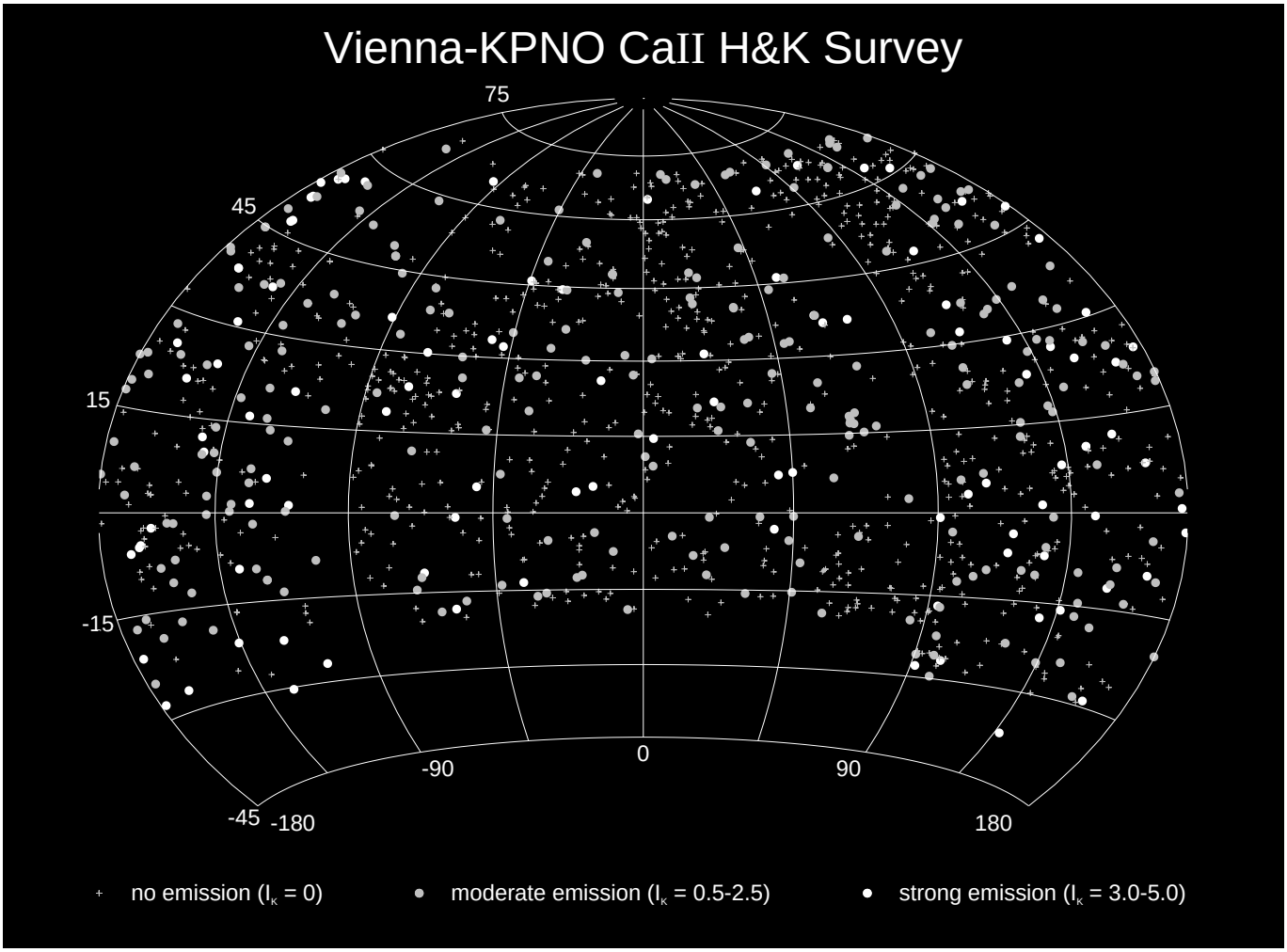

Fig. 1. The sky distribution of the sample of stars in this paper. Stars that were found to exhibit Ca II emission are shown as dots, non-emission stars as plusses. The active stars are again subdivided into weak-to-moderate emission (emission intensity, $I_{\rm K} = 0.5 - 2.5$ according to Wilson (1976) and moderate-to-strong ($I_{\rm K} = 3.0 - 5.0$) emission stars

power, $\lambda/\Delta\lambda$, as measured from the full width at half maximum (FWHM) of the thorium-argon comparison lamp lines, was 18 000 at 4020 Å and 25 000 at 6630 Å, This is an effective wavelength resolution of 0.23 Å in the blue and 0.26 Å in the red (at dispersions of 4.7 Å/mm and 7 Å/mm, respectively). The instrumental FWHM was thereby sampled by 3.2 pixels and 2.5 pixels according to slit widths of 400 μm in the blue and 280 μm in the red, respectively. Unless otherwise noted, all blue spectra were obtained with an integration time of 5 min for stars brighter than $V = 8\overset{\rm m}{.}0$, with 7 min for stars between $8\overset{\rm m}{.}0 - 8\overset{\rm m}{.}8$, and with 10 min for stars fainter than $8\overset{\rm m}{.}8$. This allows for a signal-to-noise (S/N) ratio in the continuum of approximately $20 - 40$:1. The red-wavelength spectra were obtained with integration times between 20 and 30 minutes according to S/N ratios between $70 - 150$:1. A typical spectrum for each wavelength region is shown in Fig. 3.

All spectroscopic data were reduced with IRAF and included bias subtraction, flat fielding and optimized aperture extraction. Several wavelength comparison spectra and spectra of bright radial-velocity standards were obtained during each night to ensure an accurate wavelength calibration. Twenty flat-field exposures with a tungsten reference lamp were taken at the beginning of the night and again at the end of the night. These fourty flat fields were co-added and used to remove the pixel-to-pixel variations in the stellar spectra on a nightly basis. The F3KB CCD showed no obvious signs of fringing at red wavelengths (none is expected in the blue) and no attempts were made to correct for it other than the standard flat-field division. Continuum fitting with a low-order polynomial was sufficient to find a satisfactory continuum solution. The H&K region in the blue-wavelength spectra was excluded from the continuum solution.

3.2. Photometry

Follow-up photometry of most of the stars with Ca II H&K emission was obtained with Wolfgang, one of the two 0.75-m Vienna Observatory automatic photoelectric telescopes (APTs)

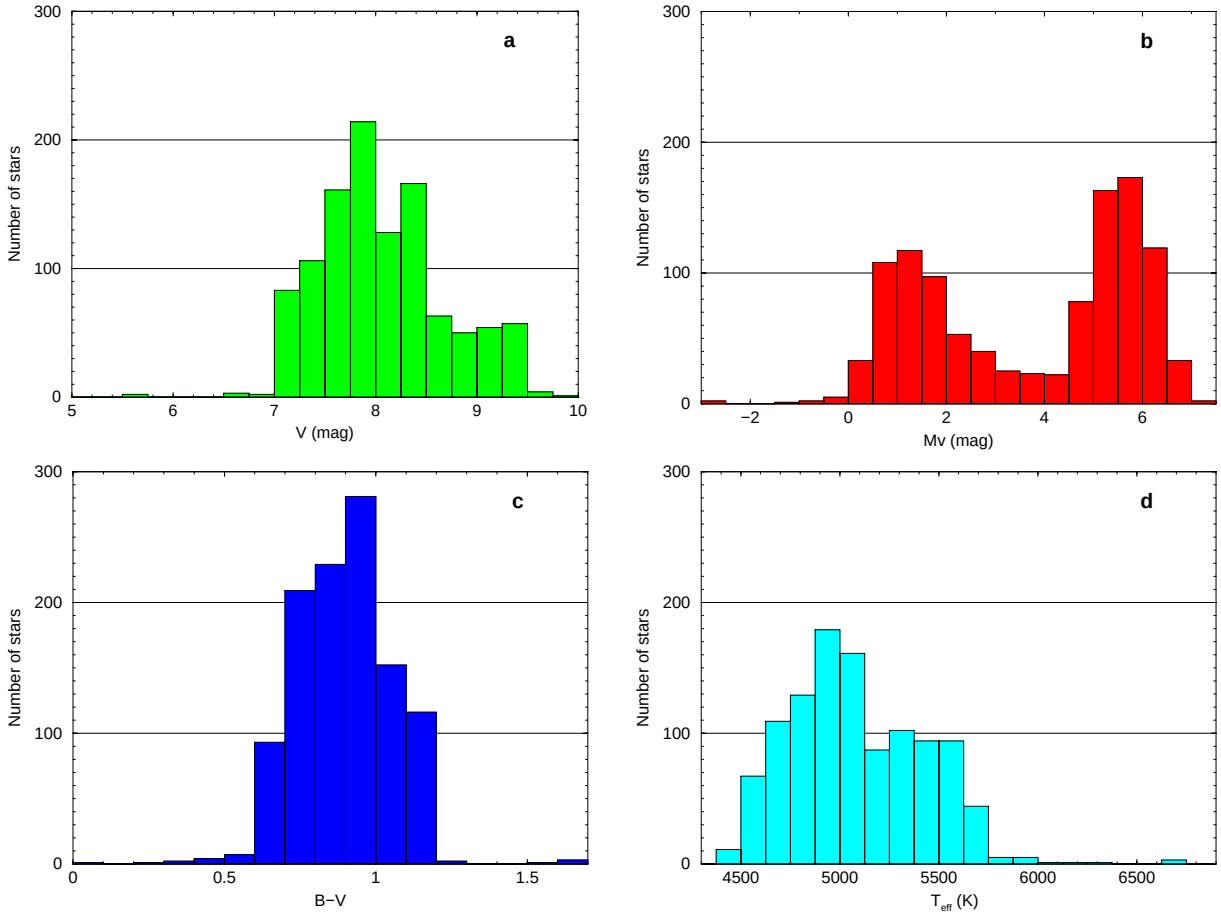

Fig. 2. Stellar parameters of the input sample. The four panels show the number of stars observed as a function of, **a)** visual brightness V, **b)** absolute magnitude M_V (based on the *Hipparcos* parallax), **c)** $B-V$ color and **d)** effective temperature $T_{\rm eff}$

at Fairborn Observatory in Arizona (Strassmeier et al. 1997b). All data were taken in and transformed to Strömgren y. Integration time was set to 20 s for each reading, except for stars fainter than $\approx 9^{\rm m}$ where 30 s were used.

Altogether, 8038 differential data points of 204 program stars are presented in this paper where each is the mean of three readings of the variable and four readings of the comparison star. This amount of data is proportional to ≈670 hours of telescope time with ≈446 hours of actual on-target integration. The observing sequence per target group was Nav-C2-Sky-C-V-C-V-C-V-C-Sky-C2 (V=Variable). A second comparison star (C2), furtherin called the check star, was observed twice per differential group. A reading on the sky was taken before and at the end of each V–C group while a bright navigation star (Nav) was recorded with the CCD finder as the first reading for each target group (these readings are for centering and are not of photometric quality). The standard error of a nightly mean from the overall seasonal mean was $0\overset{\rm m}{.}003$ in y (for more details see Strassmeier et al. 1999).

4. Results

4.1. New H&K emission-line stars and absolute surface fluxes

Absolute H&K emission-line fluxes are determined with the method of Linsky et al. (1979). It includes the measurement of the relative flux in a 50-Å band, f_{50}, between 3925 and 3975 Å and the relative flux in the H and K emission lines, $f_{\rm H}$ and $f_{\rm K}$, as defined by the $({\rm H\&K})_{\rm 1V}$ and $({\rm H\&K})_{\rm 1R}$ points, respectively. All relative fluxes are obtained by integrating the appropriate bandpass between the unnormalized spectrum and zero intensity.

The absolute emission line fluxes, $\mathcal{F}$, are calculated by comparing the ratio of the relative H&K-line flux and the relative 50-Å flux with a linear extrapolation of the absolute flux from the $V-R$ color index relation given by Linsky et al. (1979) and Strassmeier et al. (1994) and based upon the absolute photometry of Willstrop (1964):

$$\log \mathcal{F}_{50} \;=\; 8.264 - 3.076\,(V-R)_{\rm J} \qquad (1)$$

$$\mathcal{F}_{\rm H} \;=\; \frac{f_{\rm H}}{f_{50}}\,(50\,\mathcal{F}_{50}) \qquad (2)$$

$$\mathcal{F}_{\rm K} \;=\; \frac{f_{\rm K}}{f_{50}}\,(50\,\mathcal{F}_{50})\,. \qquad (3)$$

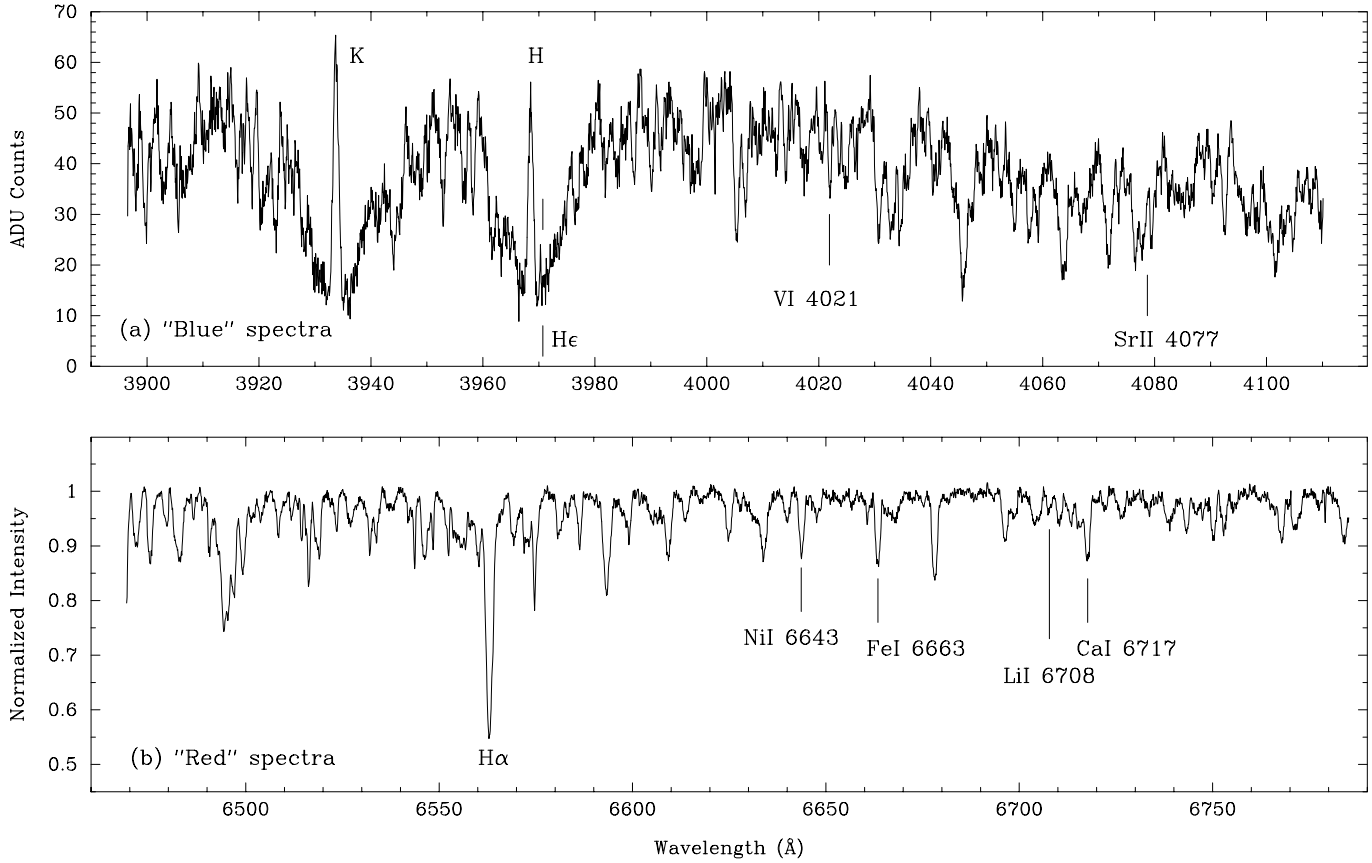

Fig. 3. Two examples of spectra obtained in this survey. Panel **a)** shows a blue-wavelength spectrum, panel **b)** a red-wavelength spectrum. Both spectra are for HD 553, a V = 8.$^{\rm m}$1 K0 (sub)giant that was discovered to exhibit strong Ca II H and K emission. The spectral lines of interest are identified

Table A1 enumerates the results of this analysis and Table 1 is a quick-look summary of the stars with H&K emission lines. In Table A1, Col. 1 lists the targets by HD number or, if unavailable, by Hipparcos number, as well as an eventual variable star name. Column 3 is the spectral classification taken from the Hipparcos-catalogue Appendix, and Col. 6 the trigonometric parallax from Hipparcos. Column 10 denotes the particular value of Johnson ($V - R$) used in Eq. (1) to transform the relative flux ratio to the absolute flux. Note that the $V - R$ colors listed are not observed values but were computed from the observed Hipparcos $B - V$ color, the deduced absolute visual brightness, and the color-color relation tabulated in Gray (1992). Using $B - V$ instead of an observed $V - R$ value minimizes the effects of cool starspots and was shown by many authors (e.g. Strassmeier et al. 1994) to be a more consistent description of the unspotted photosphere. Columns 18 and 19 list the absolute H&K emission-line fluxes and Cols. 20 and 21 the pure chromospheric fluxes. These fluxes were corrected for the photospheric contribution by subtracting the flux from a radiative equilibrium atmosphere, $\mathcal{F}^{\rm RE}_{\rm H\&K}$, given in Linsky et al. (1979) and represent the purely chromospheric emission flux, $\mathcal{F}'_{\rm H\&K}$:

$$\mathcal{F}'_{\rm H\&K} = \mathcal{F}^{\rm obs}_{\rm H\&K} - \mathcal{F}^{\rm RE}_{\rm H\&K} \ . \quad (4)$$

These fluxes may be compared with the fluxes for the non-emission stars in Table A2 as well as with the basal fluxes from Rutten et al. (1991), which are believed to be due to acoustic heating of the chromosphere. The remaining flux difference for a given spectral type is then presumably of magnetic origin. For historical reasons, we add a column, $I_{\rm K}$, to Table A1 (Col. 11) that lists the Ca II K emission-line strengths according to Wilson's (1976) 0–5 scale; 0 denotes no detectable emission, and 5 marks strong emission lines reaching the nearby continuum or above. Figure B1 in the Appendix are Ca II plots of all stars with H and K emission stronger than $I_{\rm K} \geq 1$. Furthermore, we compute the sum of the corrected fluxes in the H and K line and express it in units of the bolometric luminosity (Col. 22):

$$R_{\rm HK} = \frac{\mathcal{F}'_{\rm H} + \mathcal{F}'_{\rm K}}{\sigma\, T^4_{\rm eff}} \ . \quad (5)$$

Fourteen stars had even Hϵ in emission and we measured their absolute emission-line fluxes as well. These stars and their logarithmic Hϵ emission-line fluxes in parenthesis in erg cm^{-2} s^{-1} are: HD 553 (5.68), HIP 999 (6.57), HD 82286 (5.83), HD 95559 (6.03), HD 106855 (6.17), HD 127068 (5.92), HD 113816 (5.75), HIP 43422 (6.39), HIP 46634 (5.91), HIP 63322 (5.92), HD 145230 (5.85), HD 175742 (6.44), HD 178450 (6.52), and HD 218738 (6.43). The Ca II

emission in the spectrum of HD 127068ab can not be unambiguously assigned to one of the two components. The two different entries for the emission strength of HD 141272 are real and indicate relatively large variations of the emission-line strength. The possible triple-lined system HD 139691 (=HIP 76563; see later in Sect. 4.5) has weaker emission than the usual inclusion limit for entries in Table A1 and we list it as a non-emission star in Table A2. Also note that its spectral-type entry in the Hipparcos/Tycho catalog reads F5 while the $B-V$ entry is +1.7 $\pm$ 0.5. This indicates a composite spectrum.

Table A2 lists the results for the stars without detectable H&K emission lines (Table 2 is a summary of their most commonly used identifications). Fluxes for these stars are determined from a 1-Å band centered at the rest wavelengths of Ca II H&K, respectively. Otherwise the procedure is similar as for the emission-line stars except the subtraction of the photospheric contribution. We expect an accuracy of the absolute chromospheric fluxes for these stars of the order of $30-50\%$ based on a comparison with our previous, well-exposed KPNO spectra of γ Dor candidates (Kaye & Strassmeier 1998).

4.2. Hα morphology and absolute fluxes

The Balmer Hα line is an important indicator for chromospheric activity as well as for circumstellar emission and mass flow in late-type stars. Active stars have usually shallower Hα absorption than normal stars of similar spectral type and luminosity class while some of the very active stars of the RS CVn class even have Hα in emission. Our goal here is to verify the chromospheric nature of the Ca II H and K emission by an independent measure of the Hα core flux. We measure the inner 1-Å portion of the Hα line from our continuum-normalized spectra and then relate it to the absolute continuum flux, $\mathcal{F}_{\rm c}$, at Hα. The latter is obtained from the relations provided by Hall (1996) for various Morgan-Keenan (MK) classes:

$$\mathcal{F}_{\rm c} = 7.538 - 1.081\,(B-V) \quad (6)$$

$$\text{for MK I} - \text{V and } 0 < (B-V) < 1.4$$

$$\mathcal{F}_{\rm c} = 7.518 - 1.236\,(V-R) \quad (7)$$

$$\text{for MK V and } 0 < (V-R) < 1.4$$

$$\mathcal{F}_{\rm c} = 7.576 - 1.447\,(V-R) \quad (8)$$

$$\text{for MK I} - \text{IV and } 0 < (V-R) < 1.8.$$

We compute the continuum flux from the calibrations in Eqs. (6) and (7) and use the average value for further processing. The Hα-core flux in erg cm^{-2} s^{-1} (listed in Table A1 in Col. 24) is then computed from the measured 1-Å equivalent width under the spectrum, $W_{\rm core}$ (Col. 23 in Table A1), and zero intensity:

$$\mathcal{F}_{\rm H\alpha} = W_{\rm core}\,\mathcal{F}_{\rm c}\ . \quad (9)$$

Internal errors are estimated from repeated measurements of spectra taken during one night as well as from spectra of the same star obtained in different nights, and amount to no more than a few percent. External errors are mainly due to uncertainties in the absolute continuum flux due to errors in the colors and are estimated to be around 30%. In case the star is a double-lined spectroscopic binary, we just give the combined flux unless two values appear as separate entries in Table A1.

Out of the total of 371 H&K emission-line stars, 46 have Hα in emission or significantly filled-in by emission. The panels in Fig. B2 in the Appendix contain plots of these stars around the Hα-line region along with all other stars that have strong Ca II emission with $I_{\rm K} \geq 4$.

4.3. Lithium detections and abundances

The presence of a strong lithium line is generally a sign of stellar youth and thus indirectly also of stellar activity despite that it is still not fully clear how the lithium equivalent width relates to magnetic activity (e.g. Soderblom et al. 1993). More observations of lithium in active stellar atmospheres, especially in evolved stars that had enough time to deplete their primordial lithium, are needed to understand a possible link. In this paper, we present lithium measurements of 385 stars with H and K emission. Figure B3 in the Appendix shows plots of all stars with $W_{\rm Li} \gtrsim 10$ mÅ. Two stars (HD 144872 and HIP 82042) had an extended cosmic-ray hit at 6707.7 Å and could not be measured.

We either fit a double Gaussian or, in case the Li line is stronger than $W_{\rm Li} \approx 70$ mÅ, a single Gaussian to the Li line. In some cases we directly integrate the area under two suitably chosen continuum points. Both tasks are carried out with IRAF's `splot` routine and result in typical internal errors of $3-5\%$. However, if the Li-line strength is below ≈15 mÅ, this error increases to $10-20\%$ depending on the S/N ratio of the spectrum. Note, that the equivalent widths in Table A1 include both lithium isotopes, i.e. ^{6}Li at 6707.76 Å and ^{7}Li at 6707.91 Å but exclude the nearby Fe I 6707.443 + CN blend unless otherwise noted. This is achieved by either a double-Gaussian fit or by fitting a symmetric profile to the red side of the lithium line. We estimate the lower limit for a positive detection of lithium to approximately $2-3$ mÅ but it strongly depends on the S/N ratio of the spectrum. Because blending with the nearby Fe I line is a major source of uncertainty for measuring small lithium equivalent widths, we estimate that our values in Table A1 have external uncertainties of $5-10\%$ for $W_{\rm Li} \gtrsim$15 mÅ and $10-20\%$ for $W_{\rm Li} \lesssim$ 15 mÅ.

Lithium abundances are determined with the non-LTE curves of growth from Pavlenko & Magazzù (1996). Respective effective temperatures are adopted from the Hipparcos $B-V$ color, listed again in Table A1 for reasons of completeness, and the calibration from Flower (1996). For effective temperatures between the values for which abundances are listed in Table 1 in Pavlenko & Magazzù, we interpolate by fitting a third-order polynomial to the various entries. These abundances are uncertain by only 0.05 dex to 0.1 dex when we propogate the uncertainties from the equivalent-width measurement. If we further assume an error of $\pm$100 K for the effective stellar temperatures, the uncertainties of our abundances increase to $0.15-0.16$ dex.

Throughout this paper, we give logarithmic abundances on a scale with $\log n$(H) = 12.00. On this scale the observed

Table 1. Stars with H&K emission (data are listed in Table A1)

HD 553	HD 691	HD 745	HD 3125A	HD 4635	HD 5835	HD 5996	HD 6665	HD 6963	HD 7205
HD 7286	HD 7661	HD 7895	HD 8583	HD 8997a	HD 8997b	HD 9313	HD 9902b	HD 9902a	HD 10008
HD 12786	HD 13357B	HD 13382	HD 13507	HD 13531	HD 13579A	HD 14274	HD 14374	HD 15013	HD 16287
HD 16884	HD 17379	HD 17382	HD 18131	HD 18632	HD 18645	HD 18955b	HD 18955a	HD 19668	HD 19902
HD 19942	HD 20678	HD 21663	HD 21845	HD 23140	HD 23356	HD 23386	HD 23551	HD 24053	HD 25665
HD 25893	HD 25998	HD 26756	HD 26900	HD 27130a	HD 27130b	HD 27130	HD 27149a	HD 27149b	HD 27282
HD 27466	HD 27685	HD 27989	HD 28495	HD 29883	HD 30738	HD 31000	HD 35112	HD 37216	HD 40647
HD 40891	HD 41067	HD 41842	HD 43516	HD 43989	HD 44573	HD 45609	HD 46183	HD 46524	HD 47787
HD 50255b	HD 50255a	HD 51866	HD 52456	HD 53157	HD 53532	HD 53927	HD 54359	HD 54371	HD 56168
HD 59747	HD 60491	HD 61606	HD 61994a	HD 61994b	HD 62668	HD 64725	HD 64942	HD 65523	HD 66553
HD 69247	HD 69328	HD 69433	HD 70088	HD 70146	HD 71071	HD 71251	HD 71974	HD 72146	HD 72760
HD 73322	HD 74150	HD 75935	HD 76218	HD 76799	HD 77825	HD 78233	HD 78644	HD 79969	HD 79993
HD 80355	HD 81040	HD 81659	HD 81767	HD 82159	HD 82286a	HD 82286b	HD 82443	HD 82841	HD 82939
HD 82977	HD 83588	HD 83983	HD 85301	HD 86065	HD 86590a	HD 86590b	HD 86590c	HD 87424	HD 87547
HD 87598	HD 87883	HD 87978	HD 88638	HD 88654	HD 89546	HD 89965	HD 90442	HD 91901	HD 92945
HD 93811	HD 93915	HD 93915a	HD 93915b	HD 94765	HD 95188	HD 95559a	HD 95559b	HD 95559c	HD 95559
HD 95724	HD 95743	HD 96064	HD 96612	HD 97305	HD 97601	HD 98356	HD 99303	HD 100310	HD 101206
HD 101906	HD 102121	HD 102195	HD 102696	HD 103072	HD 103720	HD 103847	HD 104067	HD 104243	HD 104923
HD 105575a	HD 105575b	HD 105575c	HD 105631	HD 105963A	HD 105963B	HD 106023	HD 106156	HD 106453	HD 106711
HD 106855a	HD 106855b	HD 108186	HD 108564	HD 108574	HD 108575	HD 108984	HD 109011a	HD 109011b	HD 109157
HD 109647	HD 109703	HD 110463	HD 110514	HD 110833	HD 111312	HD 111487	HD 111487a	HD 111487b	HD 111813
HD 112099	HD 112733	HD 112859a	HD 112859b	HD 113247	HD 113247a	HD 113247b	HD 113449	HD 113720	HD 113816
HD 116544	HD 116956	HD 117099	HD 117860	HD 118234	HD 119332	HD 119607	HD 120205	HD 120352	HD 121629
HD 121812	HD 121979	HD 122968	HD 123351	HD 124106	HD 125874	HD 126535	HD 127068a	HD 127068b	HD 127871
HD 128165	HD 128311	HD 130004	HD 130215	HD 130307	HD 130322	HD 131023	HD 131977	HD 132425	HD 134353
HD 136378	HD 136834	HD 137778	HD 138134	HD 138157	HD 139194	HD 139837	HD 140637	HD 141071	HD 141272
HD 141919	HD 142072	HD 142680	HD 143937a	HD 143937b	HD 144087	HD 144088	HD 144872	HD 145230	HD 147776
HD 147866	HD 149028	HD 149806	HD 150202	HD 150511	HD 150748	HD 152178	HD 153525	HD 153557	HD 155712
HD 155802a	HD 155802b	HD 158972	HD 161284	HD 163621	HD 167715	HD 168603	HD 171488	HD 172393	HD 173950
HD 175742	HD 176157	HD 178450	HD 180161	HD 180263	HD 180809	HD 181219	HD 183063	HD 183870	HD 186803
HD 189087	HD 189733	HD 190470	HD 190642	HD 192263	HD 193479	HD 196795	HD 197913Aa	HD 197913Ab	HD 197913B
HD 198425	HD 199967A	HD 199967B	HD 200560	HD 200968AB	HD 201219	HD 202605	HD 203030	HD 203136	HD 205249
HD 205762	HD 206374	HD 207485	HD 207583	HD 208313	HD 208472	HD 209154	HD 209393	HD 209779	HD 210667
HD 211472	HD 214615AB	HD 214683	HD 215274	HD 215555	HD 217352	HD 217580	HD 218153	HD 218738	HD 218739
HD 220182	HD 220476	HD 221851	HD 222422	HD 223154	HD 223941	HD 224983	HD 237944a	HD 237944b	HD 237944c
HD 258857	HD 261557	HD 263175	HD 285931	HD 291095	BH Vir a	BH Vir b	CG Cyg a	CG Cyg b	HIP 999
HIP 6339	HIP 36357	HIP 39222	HIP 40774	HIP 42253	HIP 43418	HIP 43422	HIP 43751	HIP 46634	HIP 47176
HIP 50072	HIP 50660	HIP 51197	HIP 56299	HIP 57859	HIP 58560	HIP 59152	HIP 59904	HIP 63322a	HIP 63322b
HIP 63442	HIP 64059	HIP 69410	HIP 70836	HIP 75011	HIP 77179	HIP 77210a	HIP 77210b	HIP 78688	HIP 82042
HIP 83141	HIP 101227	SAO 150676a	SAO 150676b	SAO 151224a	SAO 151224b				

solar photospheric Li abundance listed by Grevesse & Anders (1991) is 1.16 $\pm$ 0.1, and the Li-6708 line appears to have an equivalent width of around 2 mÅ. This value is comparable to the detection limit from our spectra. If an entry in Table A1 is zero, then no Li above $\approx 2-3$ mÅ was detected. An entry with $\lesssim 3$ mÅ means a very weak lithium line is likely present but is unreliably small to be measured. The largest equivalent widths in our sample were measured for HD 140637 (420 mÅ), HD 6665 (398 mÅ), HD 217352 (331 mÅ) and HD 109703 (300 mÅ), which basically amount to the primordial lithium abundance. Out of the 385 stars in our (red) sample, 102 (26%) had undetectable Li, 119 (31%) had Li below 10 mÅ, 128 (33%) between $10-99$ mÅ, and 36 (9.3%) more than 100 mÅ (detections in SB2s and SB3s are counted only once). Two stars in Table A2 that have no H&K emission but were we obtained a red-wavelength spectrum seem to have significant lithium: HD 32915 with 52 mÅ ($\log n$(Li) = 1.57) and HD 123999 with 18 mÅ ($\log n$(Li) = 1.22). Both stars appear to be single.

4.4. Strontium Sr II *4077-Å line strength*

Sr II 4077 was noted to be a primary luminosity indicator for late F, G, and even K and M stars (Gray & Garrison 1989). The solar spectrum shows Sr II 4077 as a triplet line (4077.580, 4077.724, 4077.834) with a total equivalent width of 428 mÅ. However, the line is by far dominated by the 4077.724-Å transition with a low excitation potential of zero.

We fit a Gaussian or, if inappropriate due to saturation, a Voigt function to the Sr II blend and measure its equivalent width and residual intensity. Our fitting procedure minimizes the influences of the nearby La II and Cr II+Ce II blends on the blue side of the line by fitting mostly the red wing of the Sr II profile. Repeated measurements show an internal error of the equivalent width of less than 10% but continuum uncertainties, rotational broadening, low signal-to-noise ratio, and heavy blending account for an estimated external error of $\approx 20-40$%. The residual intensity, i.e. line depth measured from the continuum, is taken from the minimum of the Gaussian fit. The numerical results are listed in Table A1 and Table A2.

4.5. Radial velocities and binarity

Radial velocities were derived from the blue-wavelength spectra and the red-wavelength spectra by cross-correlating them with spectra of velocity standard stars taken during the same night. The following velocity standards were adopted from Scarfe (1990): β Oph (K2III, $v_{\rm r} = -12.18$ km s^{-1})

Table 2. Stars without H&K emission (data are listed in Table A2)

HD 15	HD 443	HD 471	HD 533	HD 629	HD 1036	HD 1059	HD 1153	HD 1241	HD 1350
HD 1426	HD 1449	HD 1605	HD 1624	HD 2034	HD 2622	HD 2712	HD 2805	HD 2814	HD 2816
HD 2841	HD 3141	HD 3250	HD 3400	HD 3681	HD 3765	HD 4029	HD 4372	HD 4388	HD 4449
HD 4561	HD 4744	HD 4754	HD 4770	HD 5035	HD 5279	HD 5349	HD 5747	HD 5873	HD 5897
HD 6360	HD 6448	HD 6555	HD 6645	HD 6890	HD 7018	HD 7149	HD 7234	HD 7385	HD 7444
HD 7639A	HD 7864	HD 7980	HD 8016	HD 8129	HD 8275	HD 8389	HD 8508	HD 8553	HD 8561
HD 8594	HD 8654	HD 8828	HD 8910	HD 9070	HD 9304	HD 9342	HD 9556	HD 9847	HD 9938
HD 10126	HD 10145	HD 10196	HD 10304	HD 10311	HD 10743	HD 10755	HD 11286	HD 11443	HD 11707
HD 11979	HD 12051	HD 12343	HD 12661	HD 13357A	HD 13783	HD 13997	HD 14204	HD 14648	HD 14787
HD 14798	HD 14855	HD 14940	HD 15014	HD 15015	HD 15096	HD 15116	HD 15299	HD 15682	HD 15734
HD 15830	HD 15851	HD 16293	HD 16366	HD 16454	HD 16559	HD 16674	HD 17190	HD 17655	HD 17673
HD 18143	HD 18175	HD 18200	HD 18916	HD 19308	HD 20165	HD 20215	HD 21774	HD 21864	HD 22233
HD 22657	HD 22854	HD 23065	HD 23439A	HD 23439B	HD 24206	HD 24238	HD 24316	HD 24467	HD 24485
HD 24604	HD 24782	HD 24964	HD 25242	HD 25347	HD 26004	HD 26334	HD 26397	HD 26465	HD 26633
HD 26634	HD 27040	HD 27115	HD 27126	HD 27235	HD 27275	HD 27574	HD 28115	HD 28172	HD 28185
HD 28338	HD 28488	HD 28821	HD 30385	HD 31439	HD 31452	HD 31865	HD 31867	HD 32237	HD 32547
HD 32915	HD 32935	HD 33142	HD 33725	HD 34101	HD 34153	HD 34616	HD 34623	HD 34839	HD 34909
HD 35518	HD 37008	HD 37986	HD 38313	HD 38904	HD 39169	HD 39847	HD 39855	HD 40708	HD 41017
HD 41196	HD 41241	HD 41303	HD 41483	HD 41785	HD 41788	HD 42182	HD 42250	HD 42532	HD 42568
HD 42606	HD 42891	HD 42983	HD 43050	HD 43062	HD 43147	HD 43188	HD 43259	HD 43306	HD 43710
HD 43944	HD 44199	HD 44263	HD 44420	HD 44671	HD 45140	HD 45231	HD 45350	HD 45652	HD 45762a
HD 45762b	HD 46090	HD 46093	HD 46375	HD 46691	HD 47157	HD 47185	HD 47186	HD 47309	HD 47955
HD 47963	HD 48238	HD 48878	HD 49027	HD 49039	HD 49116	HD 49165	HD 49566	HD 49649	HD 49674
HD 50275	HD 50590	HD 50630	HD 50662	HD 51046	HD 52145	HD 54240	HD 54401	HD 55076	HD 55255
HD 55458	HD 55647	HD 55672	HD 55893	HD 57204	HD 57470	HD 57473	HD 57678	HD 57729	HD 57758
HD 57813	HD 57901	HD 58595	HD 58662	HD 58781	HD 58899	HD 59062	HD 59560	HD 60272	HD 60299
HD 60368	HD 61145	HD 61381	HD 62676	HD 63536	HD 64114	HD 64143	HD 64211	HD 64468	HD 64490
HD 64606	HD 64921	HD 65069	HD 65371	HD 65430	HD 65562	HD 65854	HD 66046	HD 66177	HD 66221
HD 66485	HD 66509	HD 66983	HD 67740	HD 67850	HD 67960	HD 68586	HD 68638	HD 69056	HD 69076
HD 69613	HD 70352	HD 71811	HD 71887	HD 72003	HD 72614	HD 72769	HD 72946	HD 73393	HD 73512a
HD 73512b	HD 73536	HD 73667	HD 74014	HD 74377	HD 75031	HD 75073	HD 75318	HD 75697	HD 75879
HD 76294	HD 76632	HD 76752	HD 76780	HD 76844	HD 76849	HD 76909	HD 77278	HD 77338	HD 77711
HD 77712	HD 79498	HD 79581	HD 79643	HD 80131	HD 80367	HD 80448	HD 81110	HD 81438	HD 81744
HD 82460	HD 82733	HD 83804	HD 85430	HD 85916	HD 85987	HD 86661	HD 87359	HD 87680	HD 87836
HD 89023	HD 89813	HD 90107	HD 90663	HD 90711	HD 90735	HD 90812	HD 90820	HD 90932	HD 91148
HD 91299	HD 91453	HD 91527	HD 91585	HD 92048	HD 92213	HD 92320	HD 92786	HD 92788	HD 93650
HD 93800	HD 94119	HD 94164	HD 94374	HD 94718	HD 94783	HD 94880	HD 95246	HD 95848	HD 96027
HD 96460	HD 96937	HD 97004	HD 97343	HD 97658	HD 98055	HD 98078	HD 98186	HD 98281	HD 98736
HD 98839	HD 98959	HD 99994	HD 100922	HD 101227	HD 101534	HD 101728	HD 102494	HD 102800	HD 103431
HD 103432	HD 104163	HD 104782	HD 104906	HD 104988	HD 105844	HD 106495	HD 107469	HD 108849	HD 109402
HD 111285	HD 111515	HD 111978	HD 112742	HD 112758	HD 112815	HD 112914	HD 114060	HD 114125	HD 114260
HD 114783	HD 114784	HD 114823	HD 115080	HD 115153	HD 115638	HD 115755	HD 116012	HD 116056	HD 116093
HD 116442	HD 116443	HD 117635	HD 118670	HD 119585	HD 119932	HD 121129	HD 121249	HD 121320	HD 122562
HD 122676	HD 122948	HD 123265	HD 123399	HD 124292	HD 124677	HD 125056	HD 125455	HD 125920	HD 126511
HD 126532	HD 126583	HD 127352	HD 128041	HD 128356	HD 128731	HD 129674	HD 130669	HD 131509	HD 132307
HD 132756	HD 133352	HD 134043	HD 134439	HD 134440	HD 134985	HD 135725	HD 136136	HD 136274	HD 136655a
HD 136655b	HD 136894	HD 138885	HD 138919	HD 139691a	HD 139691b	HD 139691c	HD 142478	HD 143990	HD 144287
HD 144873	HD 147512	HD 149933	HD 150510	HD 150665	HD 151192	HD 151504	HD 151528	HD 151541	HD 151877
HD 152275	HD 153402	HD 154510	HD 158332	HD 159062	HD 164809	HD 164853	HD 164922	HD 164923	HD 164986
HD 165168	HD 165169	HD 165173	HD 165807	HD 166498	HD 166683	HD 167081	HD 167450	HD 167858	HD 168744
HD 168746	HD 169797	HD 169822	HD 169889	HD 170232	HD 170738	HD 171010	HD 171067	HD 171215	HD 171920
HD 172043	HD 172132	HD 172245	HD 172310	HD 172586A	HD 173399	HD 173872	HD 174000	HD 174719	HD 175516
HD 175518	HD 175905	HD 176410	HD 176646	HD 176650	HD 176733	HD 177699	HD 177778	HD 178326	HD 178473
HD 178541	HD 178848	HD 179558	HD 179722	HD 180642	HD 181007	HD 181047	HD 181098	HD 181421	HD 182293
HD 182619	HD 183098	HD 183418	HD 183993	HD 184591	HD 184592	HD 184768	HD 185055	HD 185147	HD 185353
HD 185413	HD 185527	HD 186196	HD 187000	HD 188168	HD 188386	HD 188522	HD 189751	HD 190067	HD 190404
HD 190412	HD 190536	HD 190873	HD 191425	HD 191499A	HD 191785	HD 192732	HD 192773	HD 193116	HD 193953
HD 195220	HD 195987	HD 196689	HD 196692	HD 197210	HD 197274	HD 197396	HD 197657	HD 197737	HD 198402
HD 198456	HD 198482	HD 199580	HD 199660	HD 200213	HD 200386	HD 201270	HD 201702	HD 201924	HD 202109
HD 202365	HD 202585	HD 202620	HD 202751	HD 202835	HD 202999	HD 203384	HD 203712	HD 204079	HD 204814
HD 205286	HD 205321	HD 205606	HD 206243	HD 206557	HD 206928	HD 206993	HD 207032	HD 207372	HD 207487
HD 207740	HD 207771	HD 207839	HD 207874	HD 207966A	HD 208201	HD 208398	HD 208880	HD 209181	HD 209262
HD 209776	HD 210123	HD 210144	HD 211513	HD 211642	HD 212094	HD 212291	HD 212587	HD 212771	HD 212989
HD 213012	HD 213764	HD 213786	HD 213920	HD 215097	HD 215144	HD 215152	HD 215183	HD 215500	HD 215696
HD 215704	HD 215775	HD 215886	HD 216103	HD 216259	HD 216284	HD 216560	HD 216572	HD 217635	HD 218105
HD 218220	HD 218790	HD 218949	HD 219029	HD 219202	HD 219514	HD 219670	HD 219829	HD 219920	HD 220339
HD 220658	HD 220871	HD 221194	HD 221639	HD 221822	HD 221862	HD 222405	HD 222455	HD 223070	HD 223301
HD 223302	HD 223374	HD 223498	HD 223662	HD 223847	HD 223971	HD 224116	HD 224844	HD 225004	HD 225021
HD 225170	HD 225242	HD 225261	HD 226099a	HD 226099b	HD 232118	HD 233373	HD 233389	HD 233608	HD 233826
HD 233874	HD 233882	HD 236424	HD 236427	HD 237522	HD 237707	HD 237742	HD 237960	HD 238015	HD 238130
HD 250047	HD 251383	HD 255639	HD 257886	HD 337457	HD 347850	HD 347898	31 Com	HIP 4114	HIP 8358
HIP 13338	HIP 29814	HIP 31581	HIP 34498	HIP 34866	HIP 35534	HIP 35989	HIP 36522	HIP 37146	HIP 39883
HIP 40751	HIP 42304	HIP 42491	HIP 45289	HIP 45863	HIP 46854	HIP 47975	HIP 48786	HIP 49104	HIP 50638
HIP 52782	HIP 56408	HIP 56570	HIP 59321	HIP 62911	HIP 64706	HIP 65221	HIP 65485	HIP 65837	HIP 66931
HIP 69142	HIP 76112	HIP 76566	HIP 78068	HIP 81831	HIP 83630	HIP 88208	HIP 92881	HIP 94075	SAO 45472

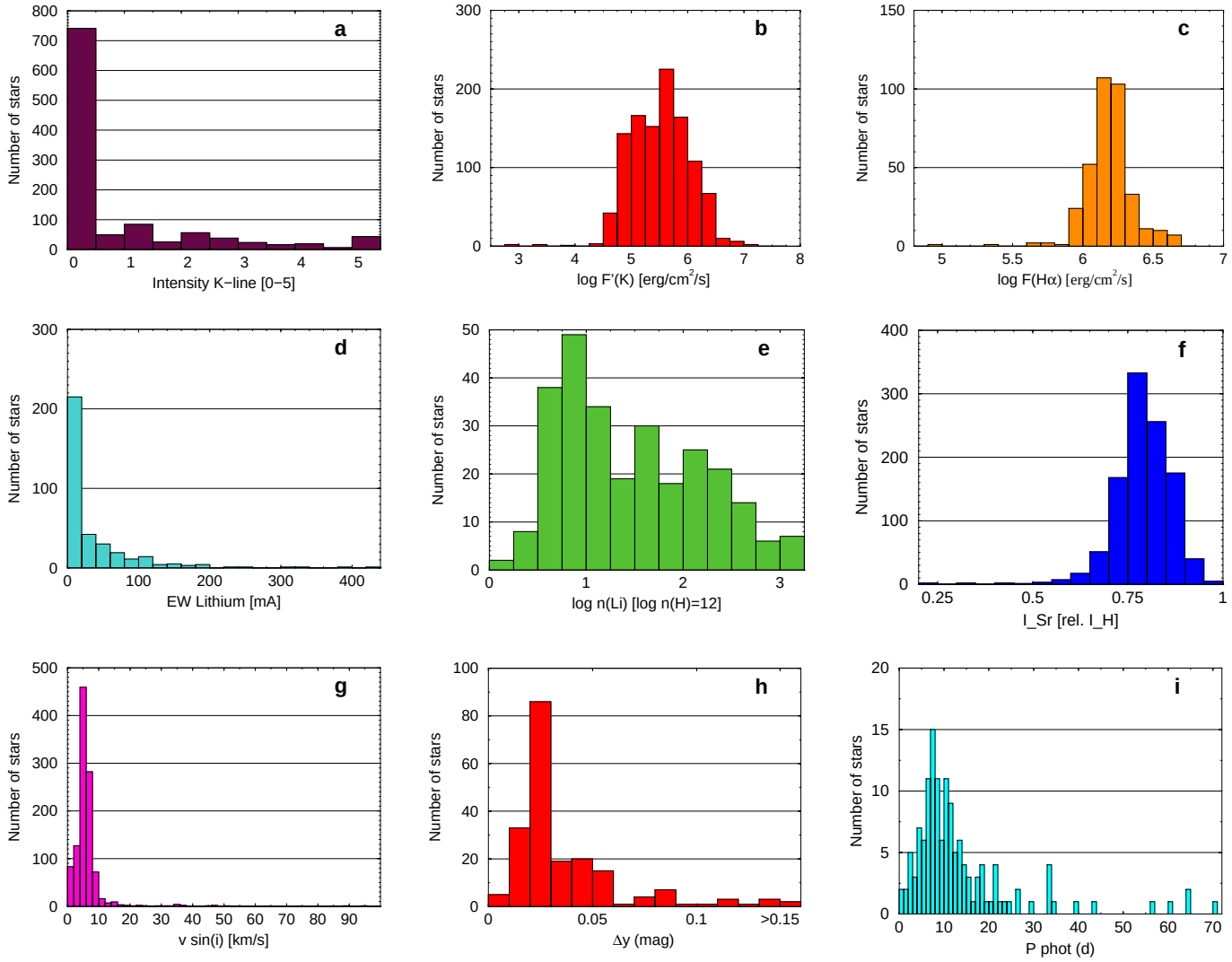

Fig. 4. Histograms for the survey results. **a)** Ca II K-line intensities ($I_{\rm K}$). The scale is from 0 (no emission) to 5 (emission at or above the continuum) according to Wilson (1976). **b)** Absolute emission-line fluxes for the Ca II-K line ($\log \mathcal{F}'(K)$). **c)** Absolute emission-line fluxes for Hα ($\log \mathcal{F}(\mathrm{H}\alpha)$). **d)** Observed Li I 6708-Å equivalent widths in milli-Å ($EW_{\rm Li}$). **e)** Logarithmic lithium abundances, $\log n(\mathrm{Li})$, in units of the hydrogen abundance ($\log n(\mathrm{H}) = 12.00$). **f)** Line-core intensity of the Sr II 4077-Å line ($I_{\rm SrII}$) with respect to the continuum. **g)** Rotational line broadening in km s^{-1} ($v \sin i$). **h)** Photometric y amplitudes in magnitudes (Δy). **i)** Rotation periods in days ($P_{\rm rot}$)

α Ari (K2IIIab, $v_{\rm r}$ = $-$14.51 km s^{-1}), β Gem (K0III, $v_{\rm r}$ = +3.23 km s^{-1}), and 35 Peg (K1III-IV, $v_{\rm r}$ = +54.26 km s^{-1}). At least two spectra of standard stars were obtained each night. All cross correlations were computed with IRAF's `fxcor` routine. It fits one or more Gaussians to the cross-correlation function in case the star is a double or triple-lined spectroscopic binary, respectively. A brief description of the measuring procedure and several applications to spotted stars were presented and discussed by Fekel et al. (1999). Several of the cross-correlation functions in the present paper appear asymmetric due to the presence of cool starspots. Measuring the velocity from a fit to the peak of the cross-correlation function would result in a less accurate velocity. Therefore, our Gaussian fits were computed to fit the entire cross-correlation profile, and not just the peak. Differences between such fits can amount to up to 3 km s^{-1} for the most asymmetric cases. Errors due to spectral-type mismatch between reference stars and program stars depend upon rotational broadening and add to the total error. Several tests with different reference stars gave negligible internal errors for $v \sin i \lesssim$ 10 km s^{-1}, approximately $\pm$0.1 km s^{-1} for $v \sin i$ up to 20 km s^{-1} and $\approx$0.3 km s^{-1} up to 50 km s^{-1}. These errors are considered small and are not included in the quoted errors in this paper. Our results are listed in Tables A1 and A2 along with the errors ($\sigma_{\rm vr}$) from the Gaussian fit. Note that the spectral region around the Ca II resonance lines ($3920 - 3980$ Å) was excluded from the blue-wavelength cross correlations, as was the Hα region ($6558 - 6568$ Å) from the red-wavelength cross correlations.

Our sample contains altogether 36 single-lined spectroscopic binaries (SB1), 17 of them are new detections (according to Simbad). The newly discovered SB1s are HD 553, HIP 999, HD 16884, HD 62668, HD 78644, HIP 46634, HD 82159, HD 82841, HIP 50072, HD 112099, HIP 63322,

HIP 63442, HD 138157, HD 142680, HD 150202, HD 153525, and HD 190642. A further 16 targets were found to be possible SB1s. In these cases the difference in velocity from the red to the blue spectrum was still larger than the sum of their uncertainties plus 1σ. These targets are HD 18645, HD 24053, HD 23551, HD 40891, HD 43516, HD 66553, HD 76799, HD 95188, HD 95724, HD 104067, HD 105963B, HD 120205, HD 147866, HD 171067, HD 184591, and HD 218739. The latter forms a visual pair with HD 218738 (=KZ And), a well-known active binary and listed in the CABS catalog.

For the cases where the cross-correlation function was double peaked, we fitted a double Gaussian to it and list the individual velocities and their errors in separate rows in Table A1 and Table A2. The stellar component with the stronger absorption lines is always called the primary (indicated by the suffix "a"). The component with the weaker line is called component "b". Altogether, 30 double-lined spectroscopic binaries (SB2) and two triple-lined spectroscopic binaries (SB3) are in our sample. The latter are HD 86590 (DH Leo), and HD 237944A. HD 237944A appears to be a newly discovered SB3 system. HD 95559, HD 139691 (ADS 9731AB) and HIP 76563 appear triple lined in the cross-correlation function from a single blue or red spectrum but that needs confirmation. At the moment, we list them as possible triple-lined systems and give three velocities in Tables A1 or A2. The double-lined systems are HD 8997, HD 9902, HD 18955, HD 27130, HD 27149, SAO 150676, SAO 151224, HD 45762, HD 50255, HD 61994, HD 73512, HIP 77210, HD 82286, HD 93915, HD 95559 (possible SB3), HD 105575, HD 106855, HD 109011, HD 111487, HD 112859, BH Vir, HD 127068, HD 136655, HD 143937, HD 155802, CG Cyg, HD 197913A, HD 199967AB, HD 202109, and HD 226099. Out of these 30 systems, 19 are new detections. The binary components of HD 199967AB are not resolved at the entrance slit and the radial velocity for component B from the blue spectrum is very uncertain due to a double-peaked cross-correlation peak. We can not decide whether it is truly doubled or just spurious. In any case, the velocity from the stronger of the two peaks is listed in Table A1 (the weaker is at 31.0 ± 5.9 km s^{-1}). The spectrum of the RS CVn binary CG Cyg (CABS # 177) appears to consist of two very broad lines at -67 ± 15 km s^{-1} and $+65 \pm 23$ km s^{-1}, respectively, and one very sharp system of lines at -0.6 ± 4.3 km s^{-1}, practically at the binary's center-of-mass velocity. The latter line system may be due to a third star but we can not exclude an absorption spectrum due to circumbinary material as suggested by Milone & Naftilan (1980). At the moment, we continue to list the star as a SB2. A similar case is HD 105575 which is classified as a β Lyrae-type eclipsing binary in Simbad. Our spectrum shows moderately strong and sharp H&K emission lines while another system of broad absorption lines is present as well. We suggest that the sharp lines are from circumbinary material and the broad lines from one of the two stellar components. Note that its Hα line appears to be tripled and shows another cross-correlation peak at 130 ± 4 km s^{-1}.

Three systems are identified with radial velocities well above 100 km s^{-1}. HD 108564, a single star with weak Ca II emission and a single velocity measure of $v_r = +111$ km s^{-1}, HD 142680, a single-lined spectroscopic binary with weak emission and two velocity measures of $v_r = -111$ and -83 km s^{-1}. It has a double-peaked cross-correlation function but the spectrum shows no clear evidence of the secondary lines. We list it as a SB1 but it could to be an unresolved SB2 system. If so, the second peak in the red spectrum gives $v_{\rm r} = -52.5 \pm 3.5$ km s^{-1}. HD 143937, a double-lined spectroscopic binary with strong Ca II emission and with peak velocities of even –166 and –170 km s^{-1} for the primary and secondary, respectively. As a comparison, a recent discovery of an extreme runaway star (HIP 60350; Maitzen et al. 1998) with +220 km s^{-1} pointed in the direction of a dynamical cluster ejection rather than to a supernovae scenario.

In case a close visual component was spatially resolved at the spectrograph entrance slit and two separate spectra were obtainable, we adopt the notation that the brighter of them is denoted component "A", and the fainter component "B". The A-component of the close visual binary HD 197913 turned out to be a SB2 with components Aa and Ab.

4.6. Space motions

Space motions are computed with the fundamental Hipparcos data (positions, distances, and proper motions) and our radial velocities. For the few entries without a Hipparcos parallax the value listed in Simbad was adopted and, if no value was listed in Simbad, we used the assigned luminosity class and the visual magnitude to determine an approximate distance (this was done for three stars: HD 9902, HD 16884, and HD 181219). No proper motions were available for HD 23386 and no distance for SAO 45472.

In case of a spectroscopic binary, or when more than one radial velocity was available, a mean was adopted. This will introduce random scatter to the space motions of the newly discovered binaries because mostly only two velocities are available and their center-of-mass velocity remains undetermined. We thus plan to interpret these data with care.

The definitions and the computing procedure for the three space-motion components (U, V, W) were outlined by Johnson & Soderblom (1987) and we basically follow their recommendations and adopt a right-handed galactic coordinate system. This makes our new values comparable to the values in the CABS catalog. The numerical values are listed in Tables A1 and A2. Again, we emphasize that for the cases of newly discovered binary systems, the observed radial velocity (or the average of the observed velocities in case the system is a SB2) are used in the computation of the space motions and not the (yet unknown) systemic velocities of the center of mass. These UVW-velocities are thus just first estimates.

Table 3. New Doppler-imaging candidates

Star	V	$\Delta V_{\rm spot}$ (mag)	Sp. type	SB?	$P_{\rm phtm}$ (days)	$v \sin i$ (km s^{-1})	Notes
HD 553	$8\overset{\rm m}{.}1$	0.05	K0III	SB1	9.06	38	=V741 Cas, eclipsing
HIP 999	8.4	0.06	G8V	SB1	1.84	20	=LN Peg (=BD+13°13)
SAO 150676	9.0	0.07	G0V+G6V	SB2	1.71	26	G6-star
HD 291095	9.0	0.25	K2−3IV	SB1	3.87	34	=V1355 Ori, not in HIP
SAO 151224a	9.3	0.15	KIV+GIV	SB2	4.98	46	eclipsing
HD 43989	8.5	0.03	G0IV	S	3.6	36	=V1358 Ori, str. Li
HD 78644	8.2	?	G3V	SB1	?	47	no photometry
HD 82286	7.9	0.13	K0IV	SB2	3.21	17/16	=FF UMa, str. Hα em.
HD 95559	9.0	0.08	<G5V>	SB2	2.94	31/26	possible triple
HD 106855	9.4	0.06	K1V	SB2	2.04	13/16	=UV Crv, Hα em.
HD 109703	8.6	0.07	G5III	S	14.2	35	very strong Li
HD 111487	9.0	0.10	G5V	SB2	1.31	36	=IM Vir, eclipsing
HD 138157	7.1	0.12	K0III	SB1	14.3	29	=OX Ser
HD 143937	8.6	0.10	<K0V>	SB2	0.913	50/43	=V1055 Sco, eclipsing
HD 145230	9.2	0.13	K2IV	SB2	12.3	19	=PX Ser
HD 152178	8.1	0.10	K0III	SB1	22.1	23	=V2253 Oph
HD 171488	7.4	0.07	G2V	S	1.337	36	=V889 Her, str. Li
HD 178450	7.8	0.10	G8V	SB1	2.13	21	=V478 Lyr
HD 190540	8.4	0.08	K0III	SB1	17.7	19	=V4091 Sgr
HD 217352	7.2	0.04	K2III	S	18.4	35	strong Li
HD 218153	7.6	0.10	K0III	SB1	25.9	24	=KU Peg

4.7. Rotational velocities

Rotational velocities, $v \sin i$, for the stars with Ca II H and K emission were determined from the widths of selected lines in the red-wavelength spectra. The procedure includes a Gaussian or Voigt fit to several unblended line profiles (mostly Ni I 6643.63 Å and Fe I 6663.45 Å) and the calibration of the average FWHM with $v \sin i$ according to the recipe of Fekel (1997). A mean macroturbulence profile and a (nightly) instrumental profile (approximated by a Gaussian) are subtracted from each FWHM measure according to Strassmeier et al. (1990). The following macroturbulence velocities were adopted: 3 km s^{-1} for solar-type dwarfs, 2 km s^{-1} for K dwarfs, 5 km s^{-1} for <G5 giants and subgiants, and 3 km s^{-1} for >G5 giants and subgiants (listed in Col. 9 in Table A1 and Table A2). Errors for $v \sin i$ from the red spectra are estimated to be $2-4$ km s^{-1} for stars with $v \sin i$ <50 km s^{-1} and ≈5 km s^{-1} for stars with higher rotation rates.

For stars without a red spectrum, i.e. the stars without Ca II H and K emission, $v \sin i$ was *estimated* from the blue spectra by measuring the FWHM of two relatively unblended lines: the V I 4020.89-Å line and the Fe I 4087.80-Åline. The final values for $v \sin i$ in Table A2 were obtained from V I because this line turned out to be less prone to blending than Fe I 4087.80-Å. Again, Fekel's (1997) relation was used for the transformation. The precision of $v \sin i$ from the blue spectra is comparably low due to the low S/N ratio and spectral resolution and is of the order of $\pm 5-8$ km s^{-1}. A correlation of $v \sin i$ from V I 4020 Å and Ni I 6643.63 Å for the stars that had a blue and a red spectrum shows no systematic deviations above the expected measuring error and a rms of $5-8$ km s^{-1}.

The results for the standard stars β Oph (K2III), α Ari (K2IIIab) and 35 Peg (K1III-IV) were 1.7 ± 1.1 km s^{-1}, 1.8 ± 1.0 km s^{-1} and 1.5 ± 1.2 km s^{-1}, respectively, and compare well with the values listed in Fekel (1997) and references therein (i.e. $1.6-2.5$ km s^{-1}, $1.8-3.1$ km s^{-1}, and 1.0 km s^{-1} for above stars, respectively).

4.8. Light curves and rotation periods

Table A3 presents the results from our photometric survey. Out of the 371 stars with Ca II H& K emission only 172 could be observed because of telescope-time limitations but 168, i.e. 97.7%, were found to be variable. A photometric period was determined for 134 of them, i.e. for 78% for the original 172 H&K emission-line stars. Lower limits for the period are found for further 11 targets. Additionally, a total of 32 of our comparison or check stars turned out to be variables and for 22 of them a possible period, or a lower limit for the period, was obtained. All periods and full y amplitudes in magnitudes are listed in Table A3 in Col. 7 and Col. 6, respectively. The periods are always given up to the last significant digit. Table A3 also gives information on the comparison and check star (Cols. 2 and 3), the JD of start and end of the observations (Cols. 4 and 5), the number of data points (Col. 8), and some individual notes (Col. 9). The full table is available electronically.

Except for a few eclipsing binaries (e.g. HD 553, HD 105575), we interpret the photometric periods found in this paper to be the stellar rotation period. Four of our target

stars were recently discovered to be variables by Cutispoto et al. (1999). For two of these stars, we obtained a first period and confirmed the periods for the other two targets. Altogether, 170 new variables were discovered. The light curves in the figures are phased with the periods from Table A3 and a zero point in time of $T_0 = 2\,451\,000$. Figure B4 in the Appendix presents the light curves for stars that have a photometric period. Figure B5 in the Appendix shows the data for stars without a period.

We applied a program that performs a multiple frequency search through Fourier transforms with a non-linear least-squares minimization of the residuals (Sperl 1998). The Fourier search range included a large number of frequencies up to the Nyquist frequency with a frequency spacing optimized for each individual data set. In most situations the frequency with the highest amplitude was adopted but, in some cases where the light curve appeared obviously double humped, twice the best-fit frequency was used. The best fits are determined by minimizing the squares of the residuals between trial fits and measurements. Further details on the period analysis can be found in Strassmeier et al. (1999).

To judge the significance of certain frequency peaks we compute a running mean of the frequency distribution for a signal-to-noise ratio of 4:1 which was found empirically by Breger et al. (1993) to indicate the limit for a significant period. From numerical simulations with varying amounts of white noise, Kuschnig et al. (1997) showed that frequency peaks with $S/N \geq 4.0$ suggest a 99.9% probability for a real period. Furthermore, since we interpret the photometric period to be the stellar rotation period, a particular period must be in agreement with the spectroscopically measured $v \sin i$ and an assumed stellar radius according to the adopted spectral classification. This reduces the range of possible periods significantly.

5. Summary

Figure 4 summarizes the statistics of the survey results. A series of histograms show the distribution of the numerical values of nine activity indicators. Out of the total of 1058 stars observed, 371 (35%) were found with Ca II H&K emission but only 78 (7.3%) with $v \sin i \geq 10$ km s^{-1}. On the contrary, a lithium line was detected in 283 (74%) of all stars that had Ca II emission (with 58% of the stars with lithium above 10 mÅ). Out of a subsample of 172 stars with moderate to strong Ca II emission, 168 (97.7%) turned out to be photometric variables and for 134 a photometric (i.e. rotation) period could be obtained. Stellar activity, rotational broadening of spectral lines, and knowledge of a precise stellar rotation period are the key requirements for Doppler imaging. Table 3 lists our new candidates for observation with this technique. Three of the candidates, HD 218153, HD 171488 and HD 291095, were already observed with high-resolution spectroscopy and are currently being Doppler imaged by the authors. In a forthcoming second part of the analysis, we will consider relations between the various activity indicators as deduced from the observations in this paper.

Acknowledgements. KGS is very grateful to the *Austrian Fond zur Förderung der wissenschaftlichen Forschung* for support through grants S7302-AST (Doppler imaging) and S7301-AST (APT). We all wish to thank NOAO/KPNO for devoting generous amounts of coudé-feed telescope time to fundamental spectroscopy of active stars. We also appreciate numerous discussions with Dr. F.C. Fekel (TSU) regarding our targets and with Dr. J.B. Rice regarding the applicability of the Doppler-imaging technique. This research has made extensive use of the Simbad database, operated at CDS, Strasbourg, France.

References

Balona L.A., 1987, SAAO Circ. 11, 1
Bidelman W.P., 1954, ApJS 1, 175
Bidelman W.P., 1981, AJ 86, 553
Bidelman W.P., 1983, AJ 88, 1182
Bidelman W.P., 1985, AJ 90, 341
Bidelman W.P., 1988, PASP 100, 1084
Bidelman W.P., MacConnell D.J., 1973, AJ 78, 687
Breger M., Stich J., Garrido R., et al., 1993, A&A 271, 482
Buzasi D.L., 1999, in Pallavicini R. (ed.), Stellar Clusters and associations: convection, rotation, and dynamos, Euroconference, Palermo, PASPC (in press)
Cutispoto G., Pastori L., Tagliaferri G., Messina S., Pallavicini R., 1999, A&AS 138, 87
Duncan D.K., Vaughan A.H., Wilson O.C., et al., 1991, ApJS 76, 383
ESA, 1997, The Hipparcos and Tycho catalogue, SP-1200
Fekel F.C., 1997, PASP 109, 514
Fekel F.C., Balachandran S., 1993, ApJ 403, 708
Fekel F.C., Moffett T.J., Henry G.W., 1986, ApJS 60, 551
Fekel F.C., Strassmeier K.G., Weber M., Washuettl A., 1999, A&AS 137, 369
Flower P.J., 1996, ApJ 469, 355
Gray D.F., 1992, The observation and analysis of stellar photospheres. CUP, Cambridge, p. 430
Gray R.O., Garrison R.F., 1989, ApJS 69, 301
Grevesse N., Anders E., 1991, in Cox A.N., et al. (eds.), Solar Interior and Atmosphere. The Univ. of Arizona Press, Tucson, p. 1227
Hall J.C., 1996, PASP 108, 313
Henry T.J., Soderblom D.R., Donahue R.A., Baliunas S.L., 1996, AJ 111, 439
Johnson D.H., Soderblom D.R., 1987, AJ 93, 864
Kaye A.B., Strassmeier K.G., 1998, MNRAS 294, L35
Kuschnig R., Weiss W.W., Gruber R., Bely P.Y., Jenkner H., 1997, A&A 328, 544
Lastennet E., Freire Ferrero R., 1994, A&AS 108, 611
Linsky J.L., Worden S.P., McClintock W., Robertson R.M., 1979, ApJS 41, 47
Lloyd-Evans T., Koen M.C.J., 1987, SAAO Circ. 11, 21
Maitzen H.M., Paunzen E., Pressberger R., Slettebak A., Wagner R.M., 1998, A&A 339, 782
Milone E.F., Naftilan S.A., 1980, in Plavec M.J., Popper D.M., and Ulrich R.K. (eds.), Close Binary Systems: Observations and Interpretations, IAU Symp. 88. Reidel, Dordrecht, p. 419
Noyes R.W., Hartmann L.W., Baliunas S.L., Duncan D.K., Vaughan A.H., 1984, ApJ 279, 763
Pavlenko Ya.V., Magazzù A., 1996, A&A 311, 961
Rice J.B., 1996, in Strassmeier K.G. & Linsky J.L. (eds.), IAU Symp. 176, Stellar Surface Structure. Kluwer, Dordrecht, p. 19

Rutten R.G.M., Schrijver C.J., Lemmens A.F.P., Zwaan C., 1991, A&A 252, 203
Scarfe C.D., Batten A.H., Fletcher J.M., 1990, Publ. Dominion Ap. Obs. 18, No. 2, 21
Schrijver C.J., 1996, in Strassmeier K.G. & Linsky J.L. (eds.), IAU Symp. 176, Stellar Surface Structure. Kluwer, Dordrecht, p. 1
Soderblom D.R., Jones B.F., Balachandran S., Stauffer J.R., Duncan D.K., Fedele S.B., Hudon J.D., 1993, AJ 106, 1059
Soderblom D.R., King J.R., Henry T.J., 1998, AJ 116, 396
Solanki S., Motamen S., Keppens R., 1997, A&A 324, 943
Sperl M., 1998, Commun. Astroseismology 111, 1
Stix M., 1989, The Sun, A&A Library. Springer, Berlin
Strassmeier K.G., 1994, A&AS 103, 413
Strassmeier K.G., Bartus J., Kövari Z., Weber M., Washuettl A., 1998, A&A 336, 587
Strassmeier K.G., Bartus J., Rodonó M., Cutispoto G., 1997a, A&AS 125, 11
Strassmeier K.G., Boyd L.J., Epand D.H., Granzer Th., 1997b, PASP 109, 697
Strassmeier K.G., Fekel F.C., Bopp B.W., Dempsey R.C., Henry G.W., 1990, ApJS 72, 191
Strassmeier K.G., Hall D.S., Fekel F.C., Scheck M., 1993, A&AS 100, 173
Strassmeier K.G., Handler G., Paunzen E., Rauth M., 1994, A&A 281, 855
Strassmeier K.G., Serkowitsch E., Granzer Th., 1999, A&AS 140, 29
Willstrop R.V., 1964, MRAS 69, 83
Wilson O.C., 1976, ApJ 205, 823

Appendix A: Tables

Table A1 lists the results for stars that were found to exhibit H&K emission while Table A2 lists the results for stars without detectable H&K emission. Table A3 summarizes the results from the photometric monitoring. All tables are available only in electronic form.

Appendix B: Figures

The following five figures show the spectra for the H&K emission-line stars in the wavelength region around Ca II H and K (Fig. B1). A subsample of the stars with strong Ca II emission is plotted in the Hα region (Fig. B2) and in the lithium region at 6708 Å (Fig. B3). The Strömgren y photometry is shown in Figs. B4 and B5 (Fig. B4 is for the stars with a photometric period and Fig. B5 for those without a detectable period).

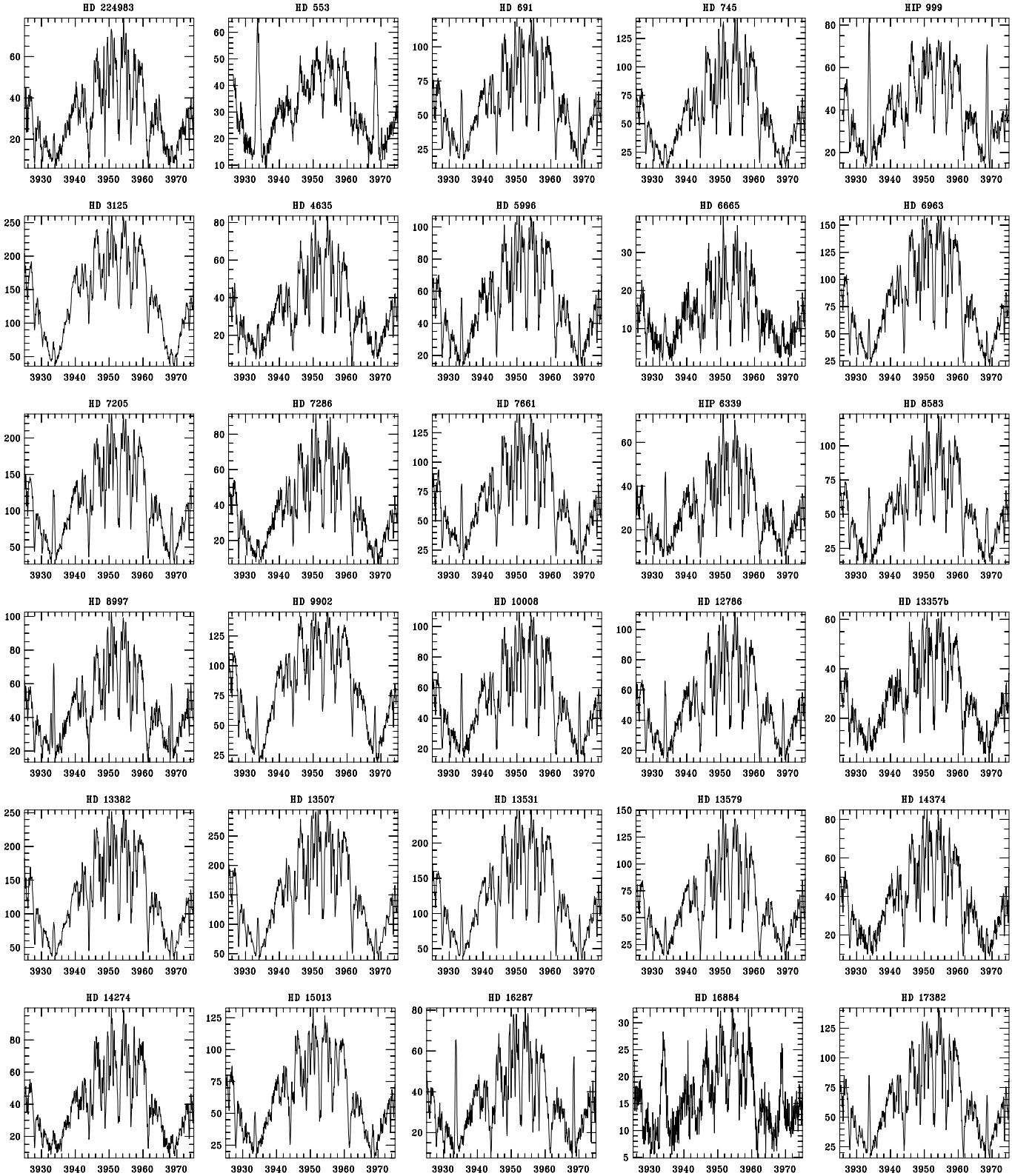

Fig. B1. Ca II spectra of stars with H and K emission. Shown are the 316 stars with an intensity level in the K line of $I_{\rm K} \geq 1$. The HD number (or HIP number or Variable Star designation if no HD number exists) is identified on top of each plot. Each plot covers a range of 50 Å centered at 3950 Å

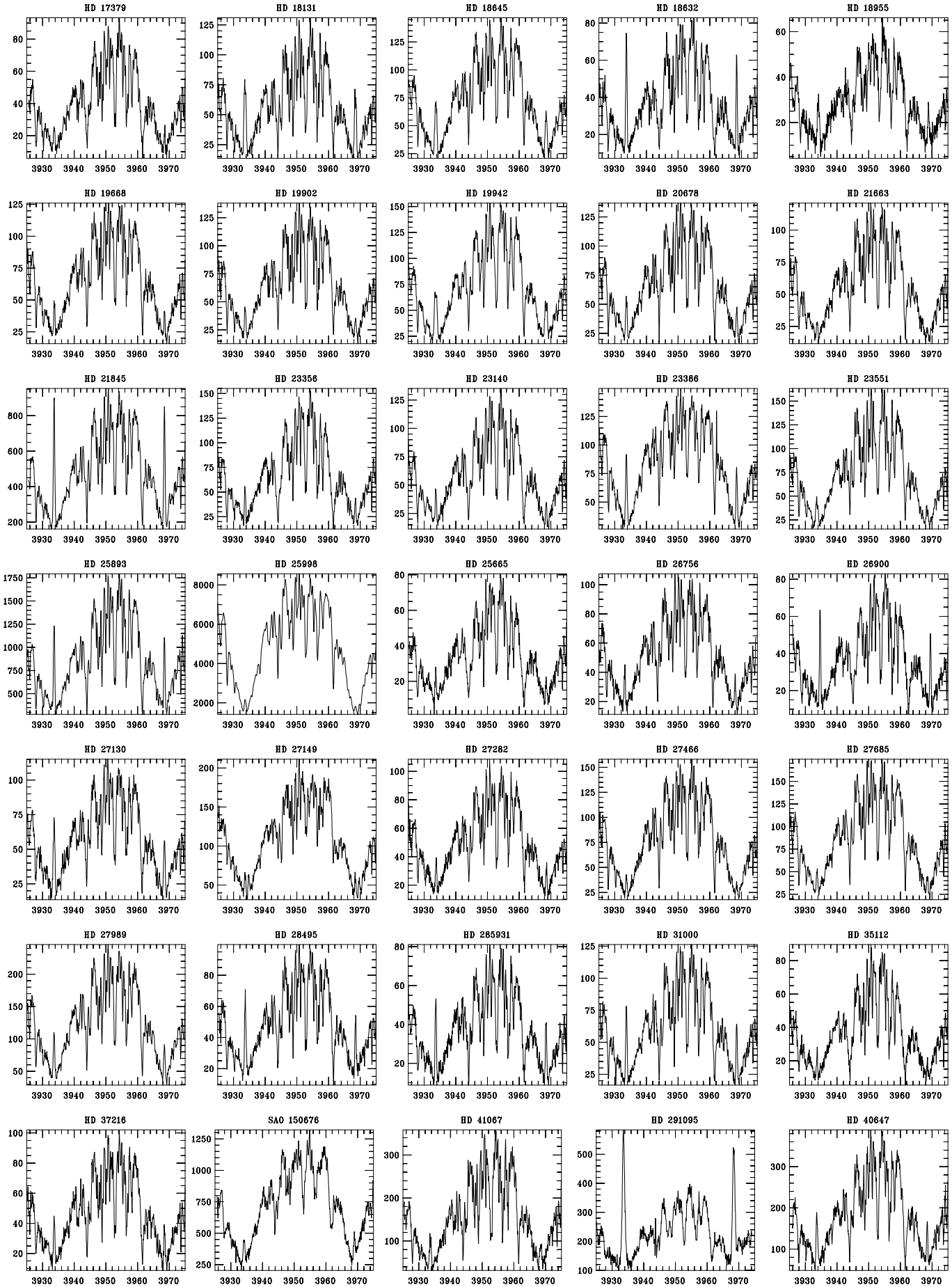

Fig. B1. continued

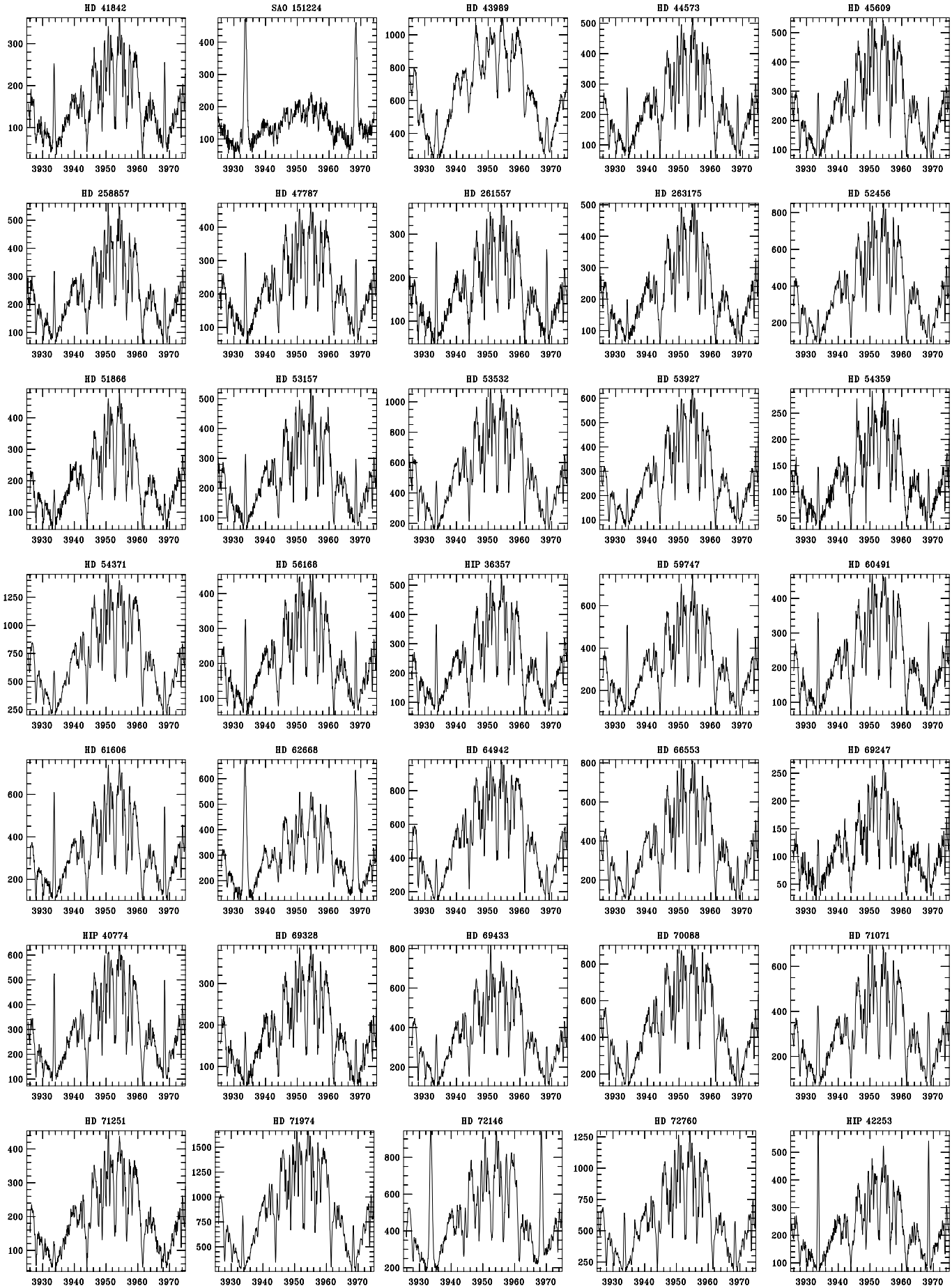

Fig. B1. continued

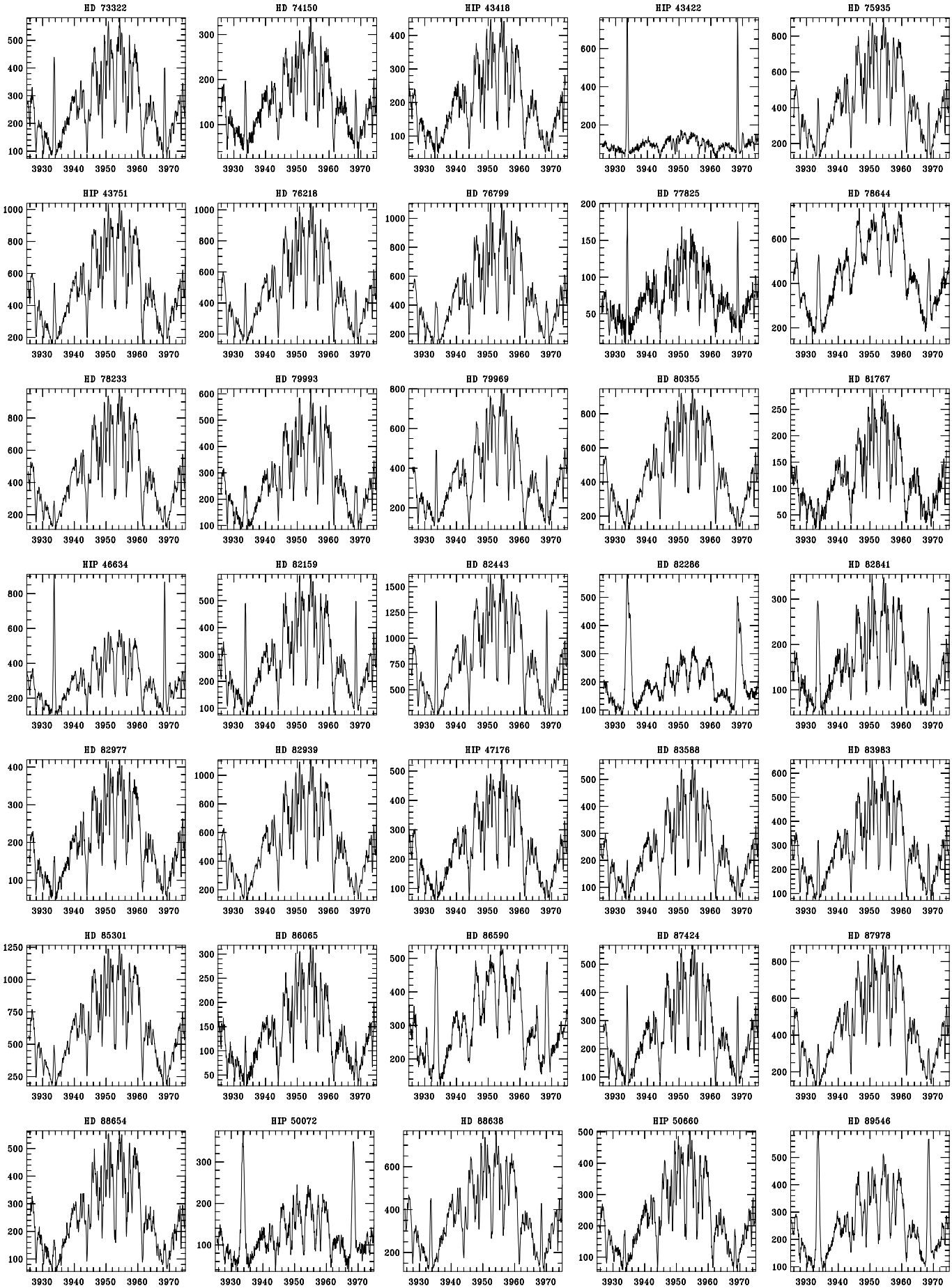

Fig. B1. continued

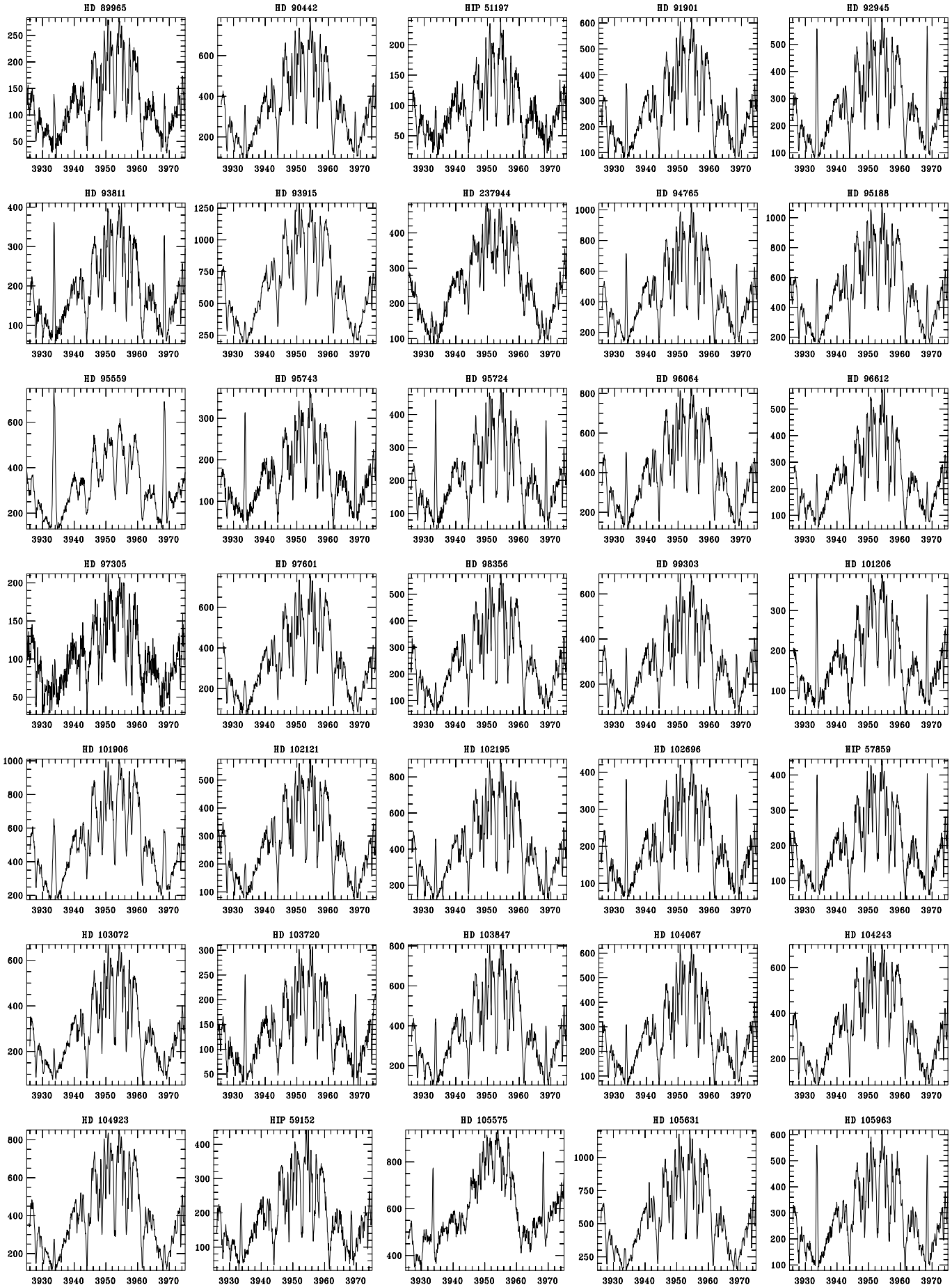

Fig. B1. continued

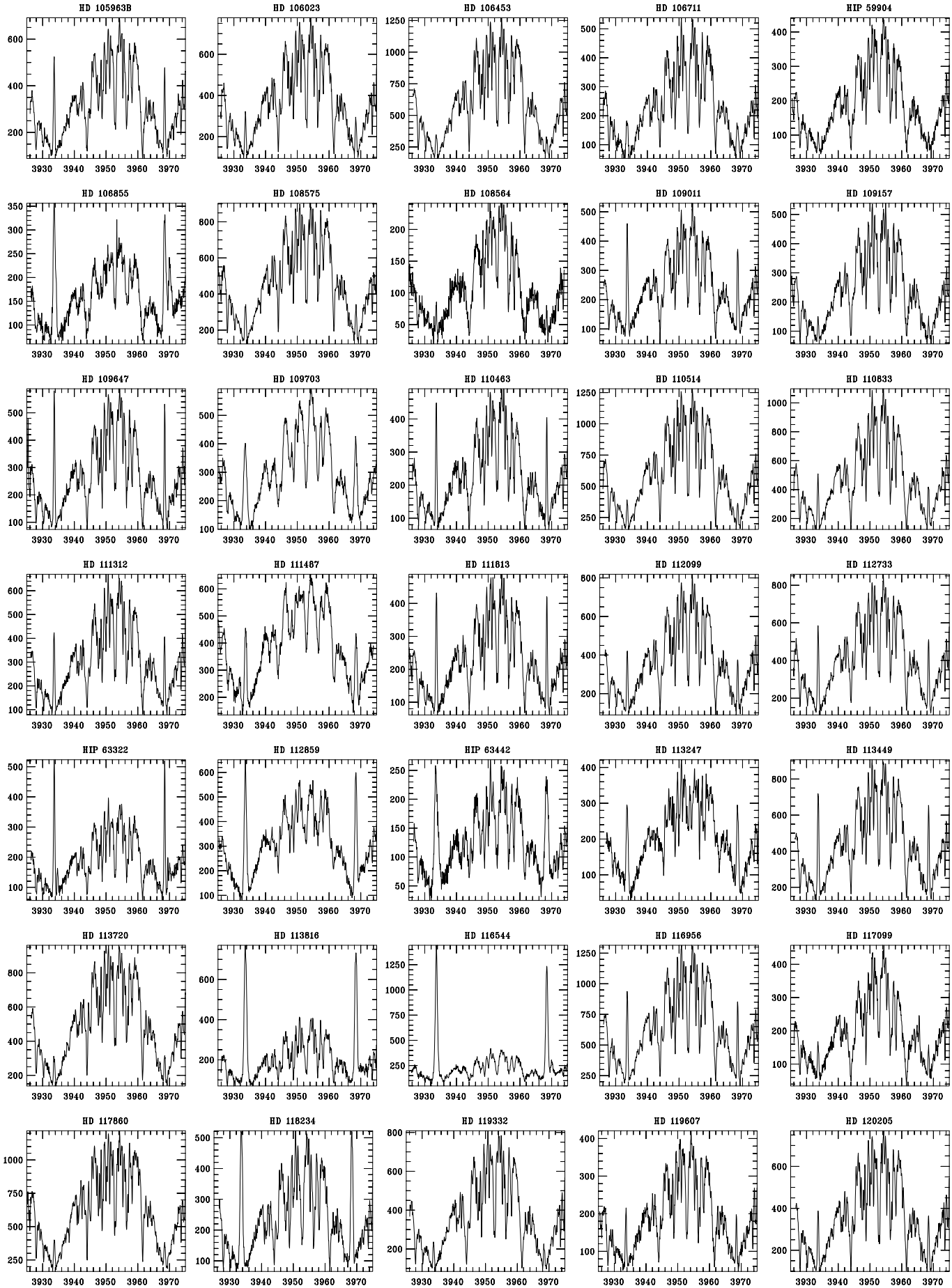

Fig. B1. continued

Next File

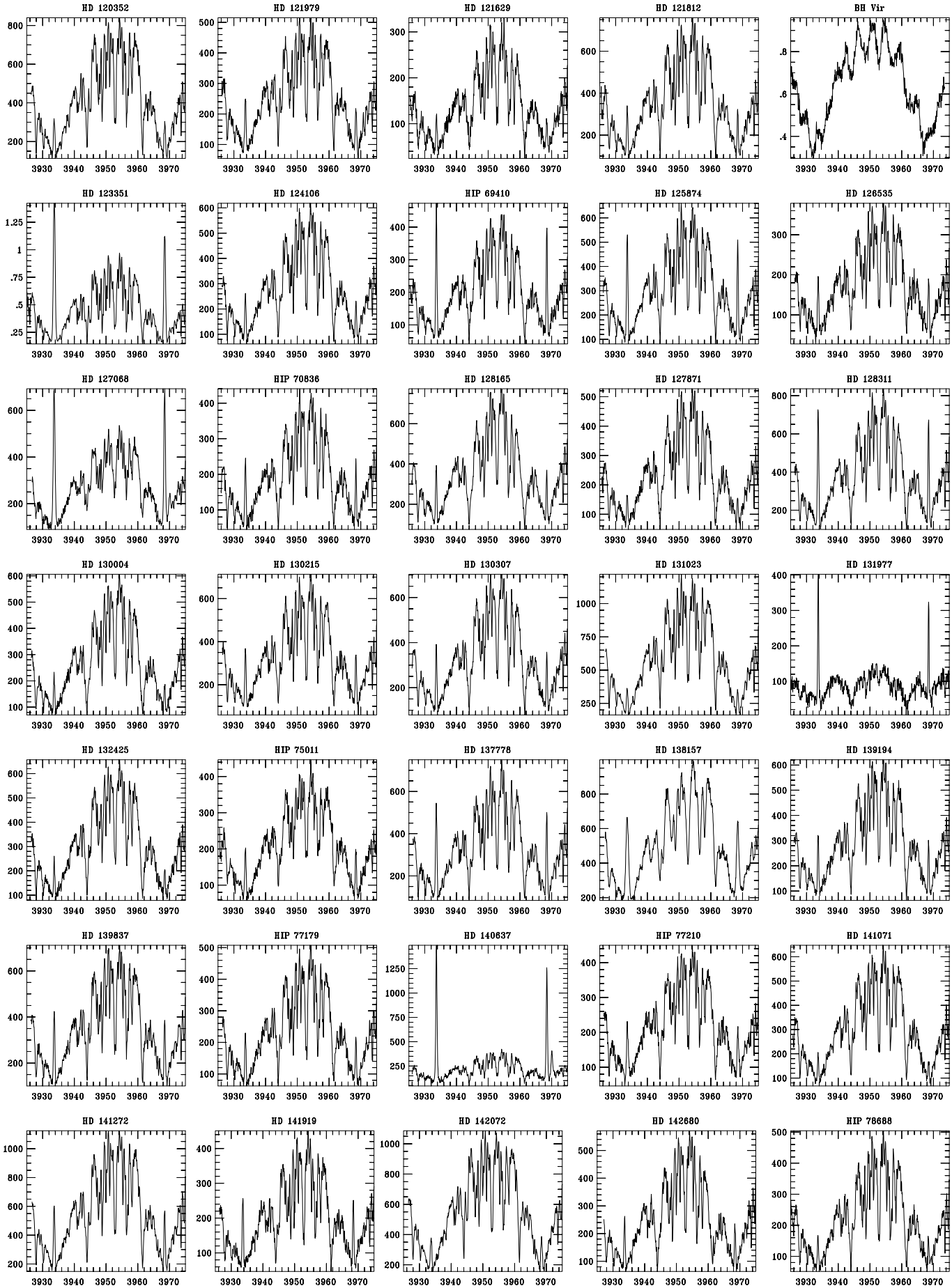

Fig. B1. continued

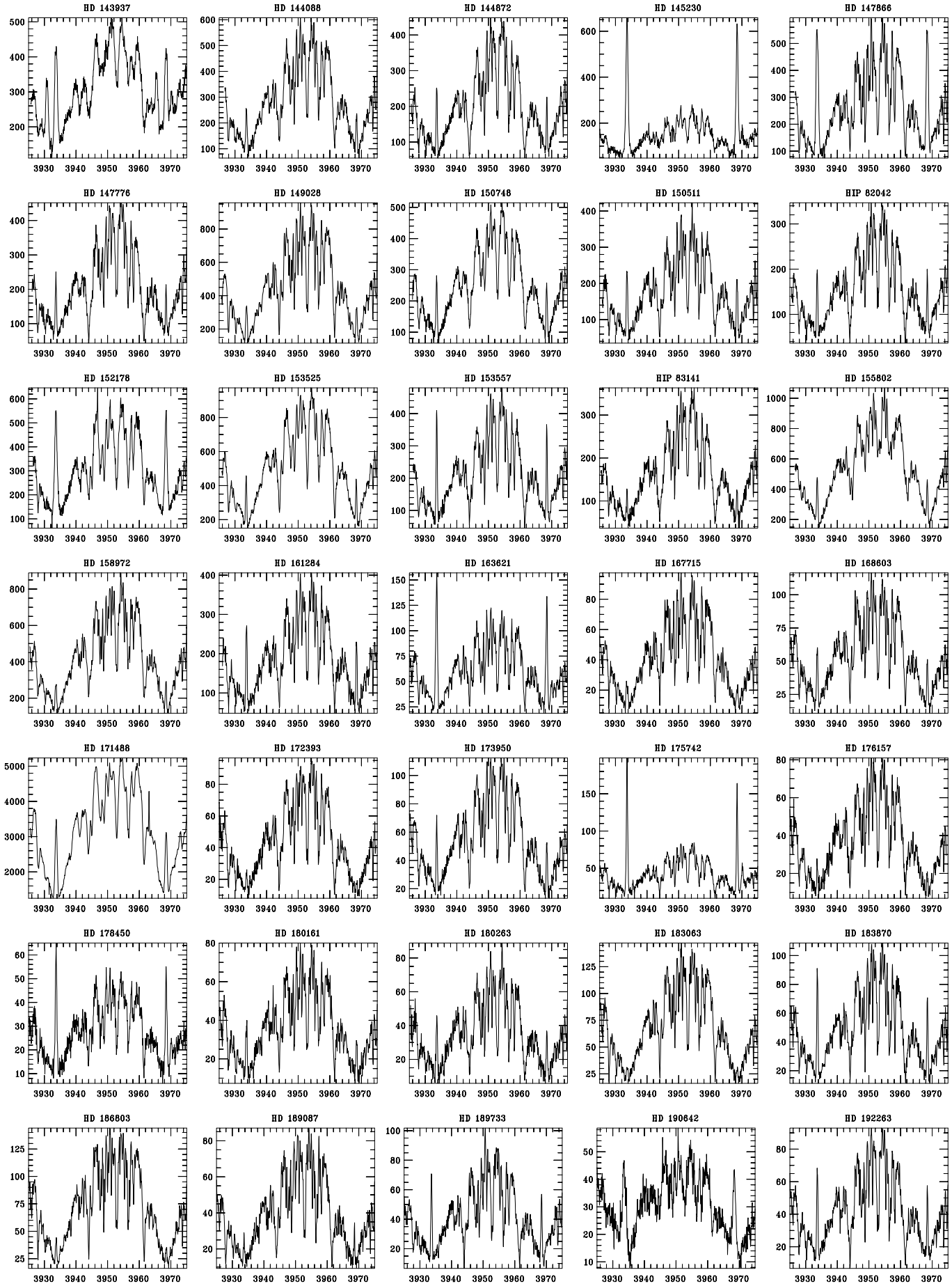

Fig. B1. continued

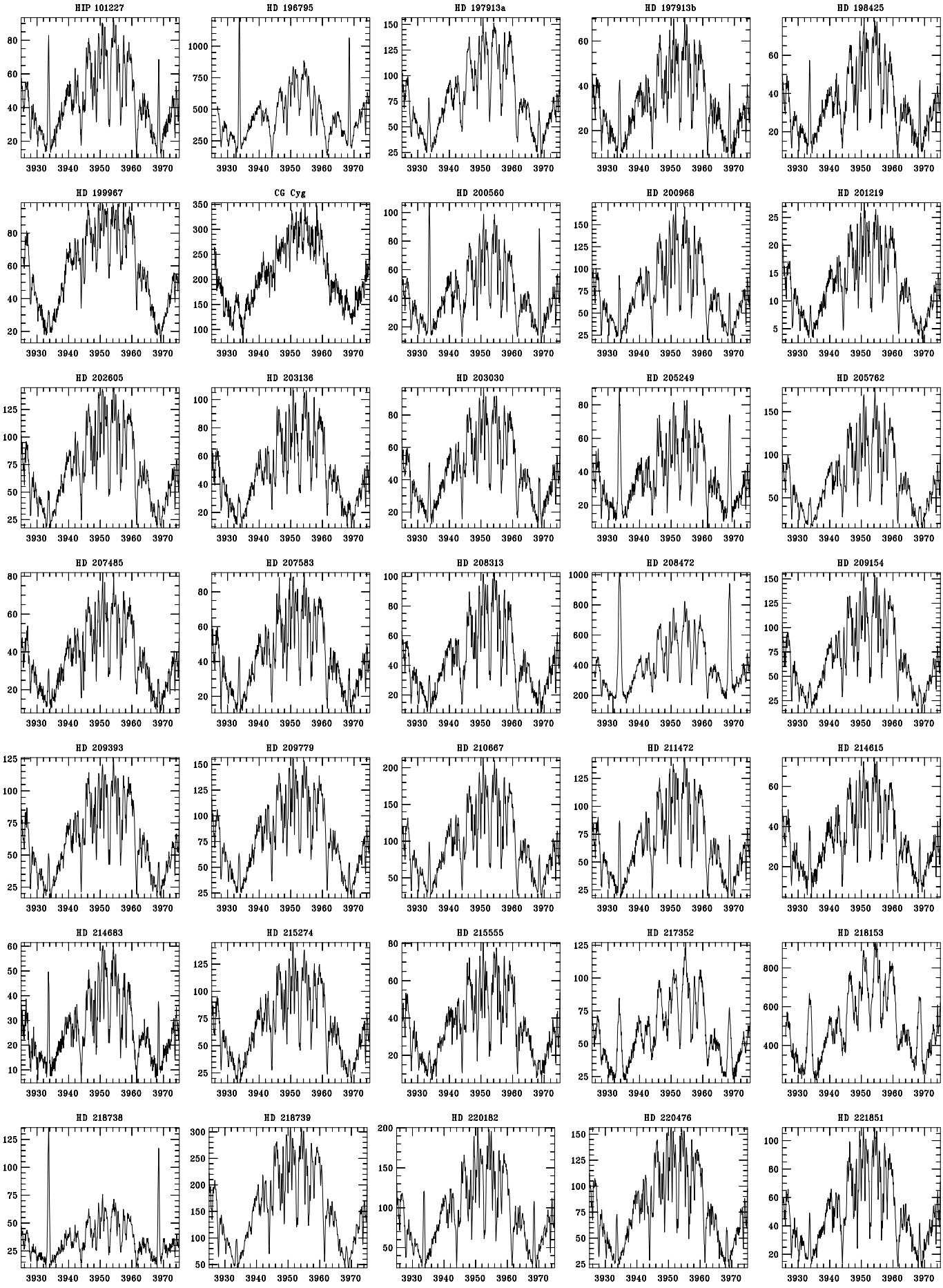

Fig. B1. continued

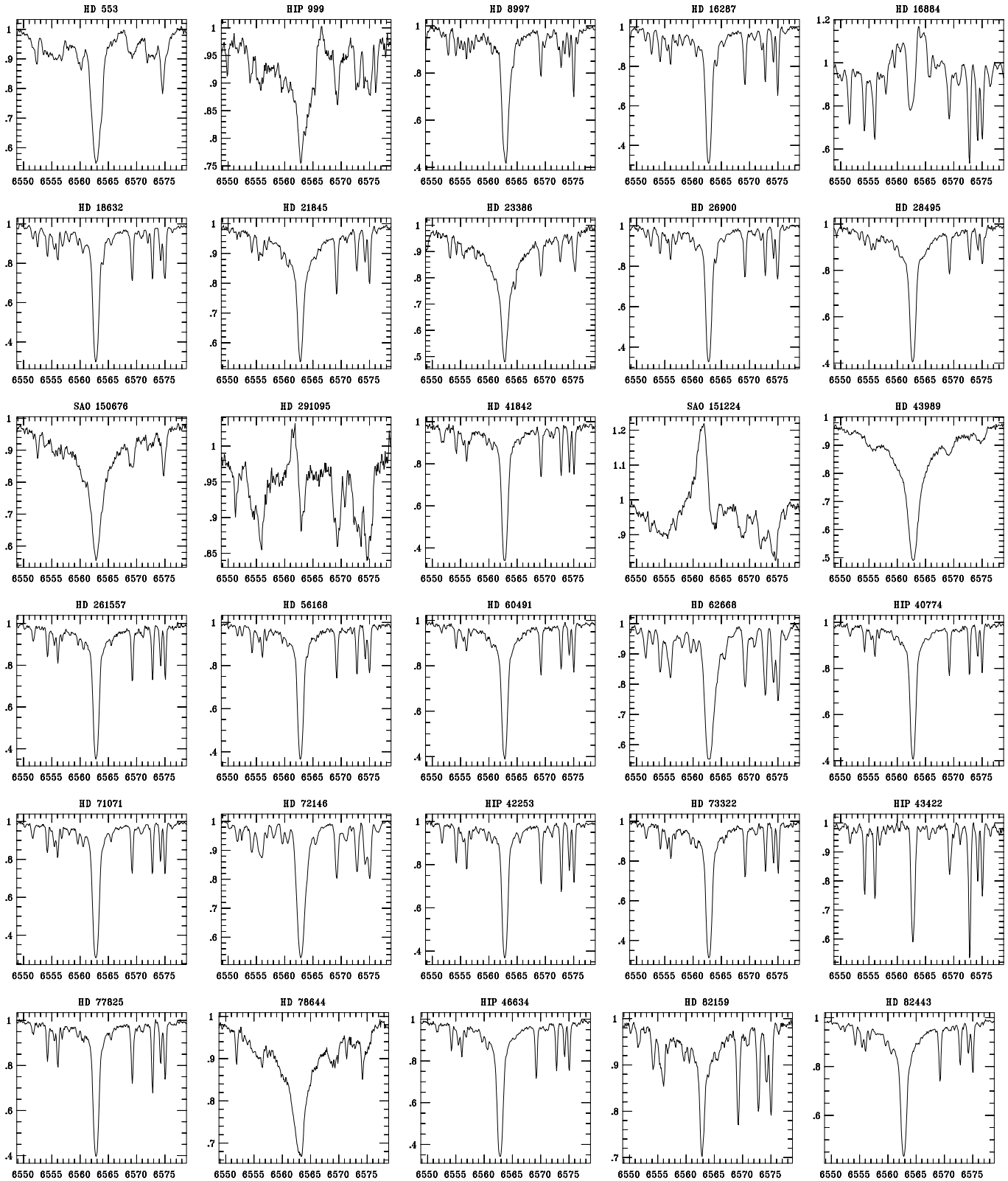

Fig. B2. Selected Balmer Hα spectra of stars with strong Ca II H and K emission. The HD number (or HIP number if no HD number exists) is identified on top of each plot. The wavelength range shown is 30 Å

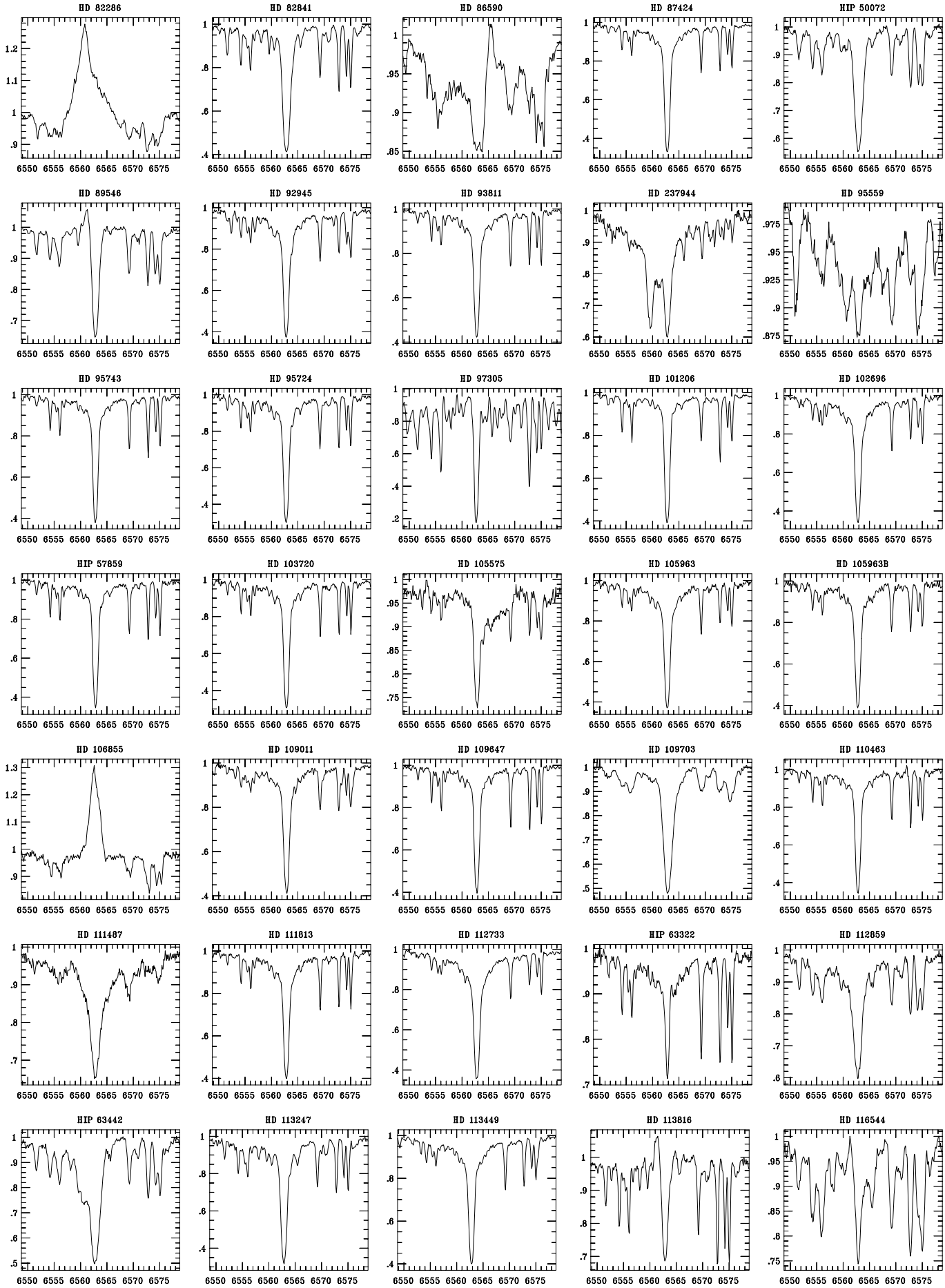

Fig. B2. continued

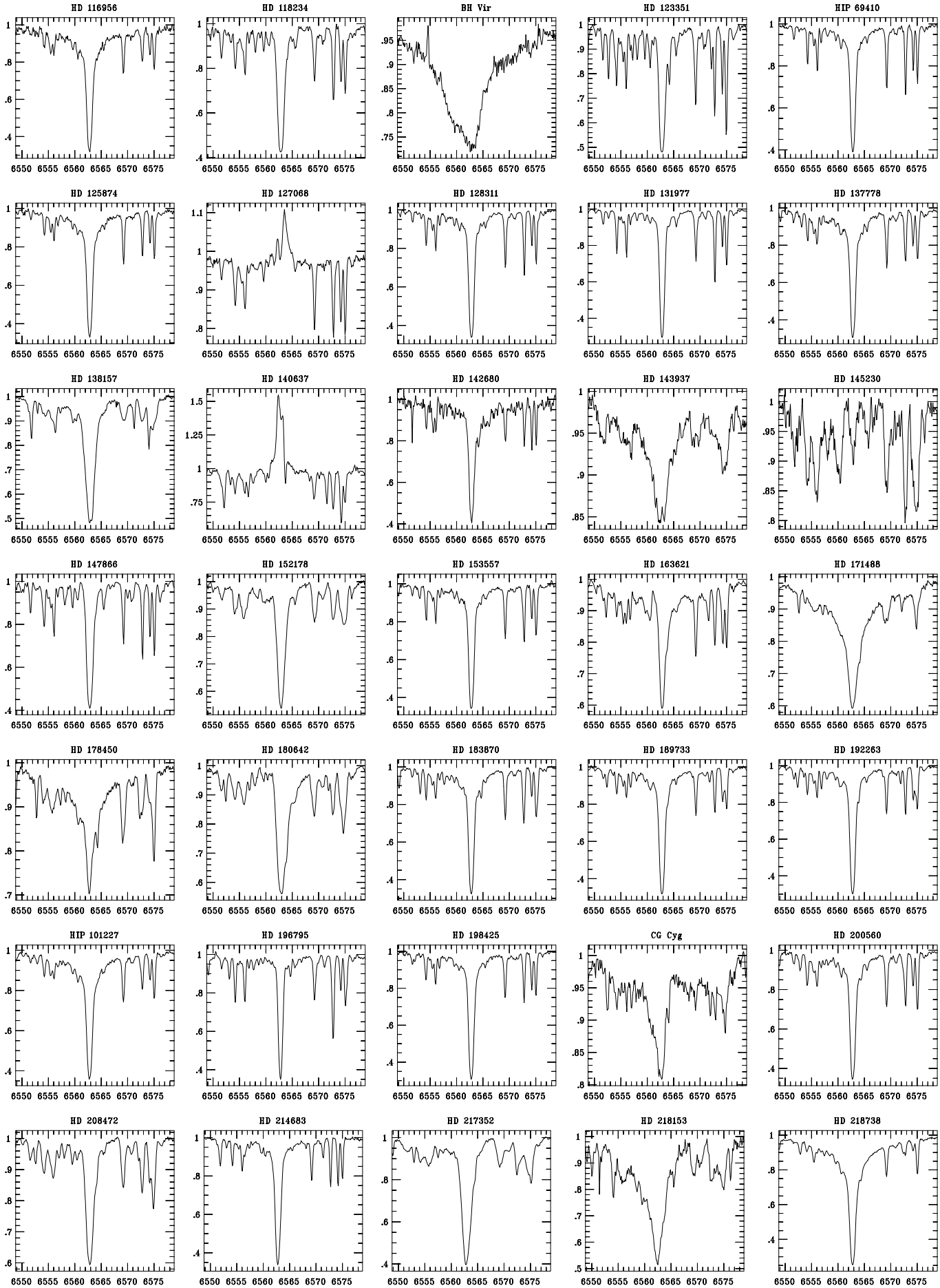

Fig. B2. continued

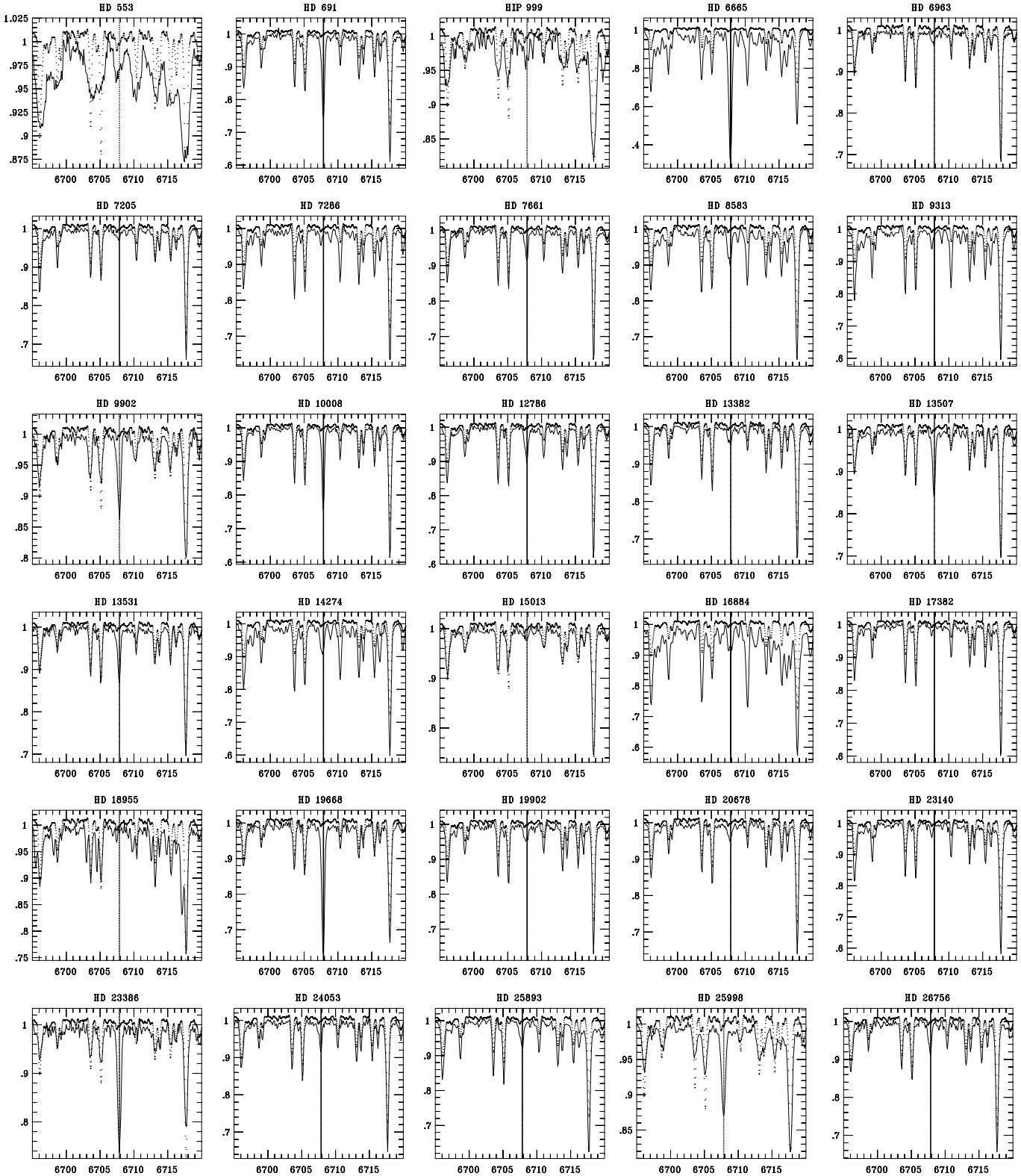

Fig. B3. Lithium 6707.8-Å spectra of stars with Ca II H and K emission and $W_{\rm Li} \geq 10$ mÅ. The HD number (or HIP number if no HD number exists) is identified on top of each plot. The wavelength range shown is 25 Å. The dotted spectrum is a spectrum of the Sun vertically shifted by 0.01 for comparison purposes (the solar lithium equivalent width is ≈2 mÅ). The vertical line is the average rest wavelength of Li I at 6707.8 Å

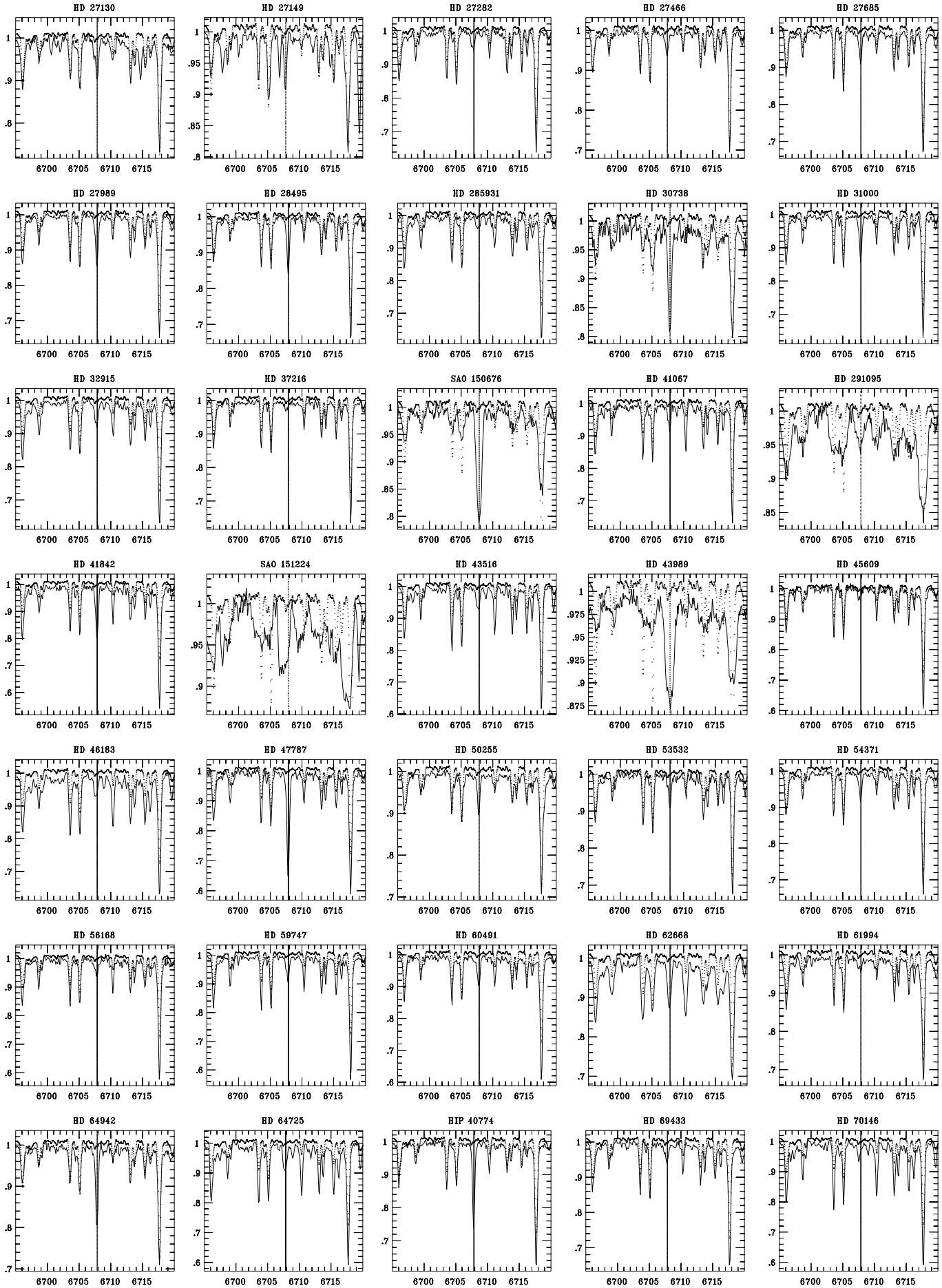

Fig. B3. continued

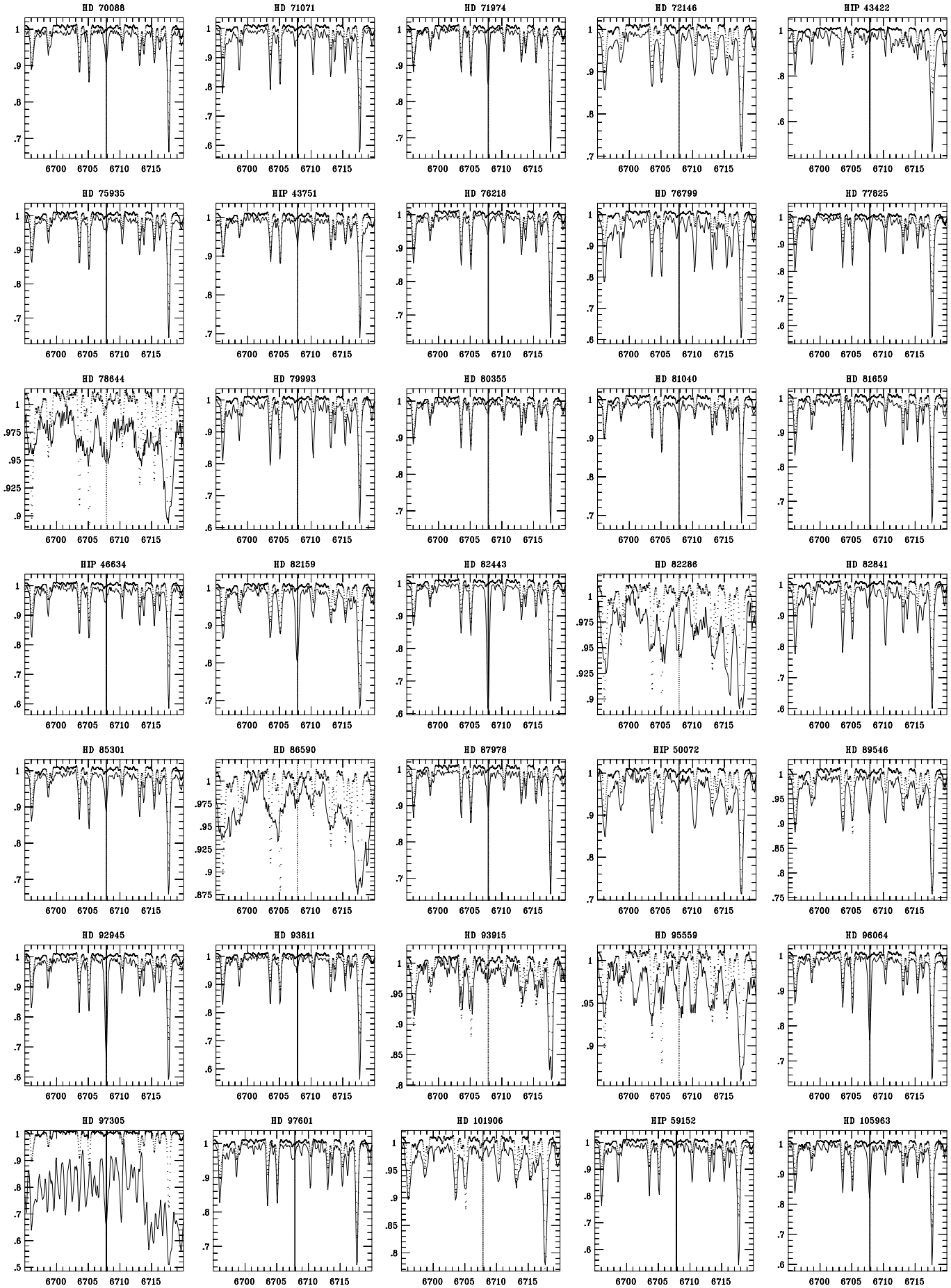

Fig. B3. continued

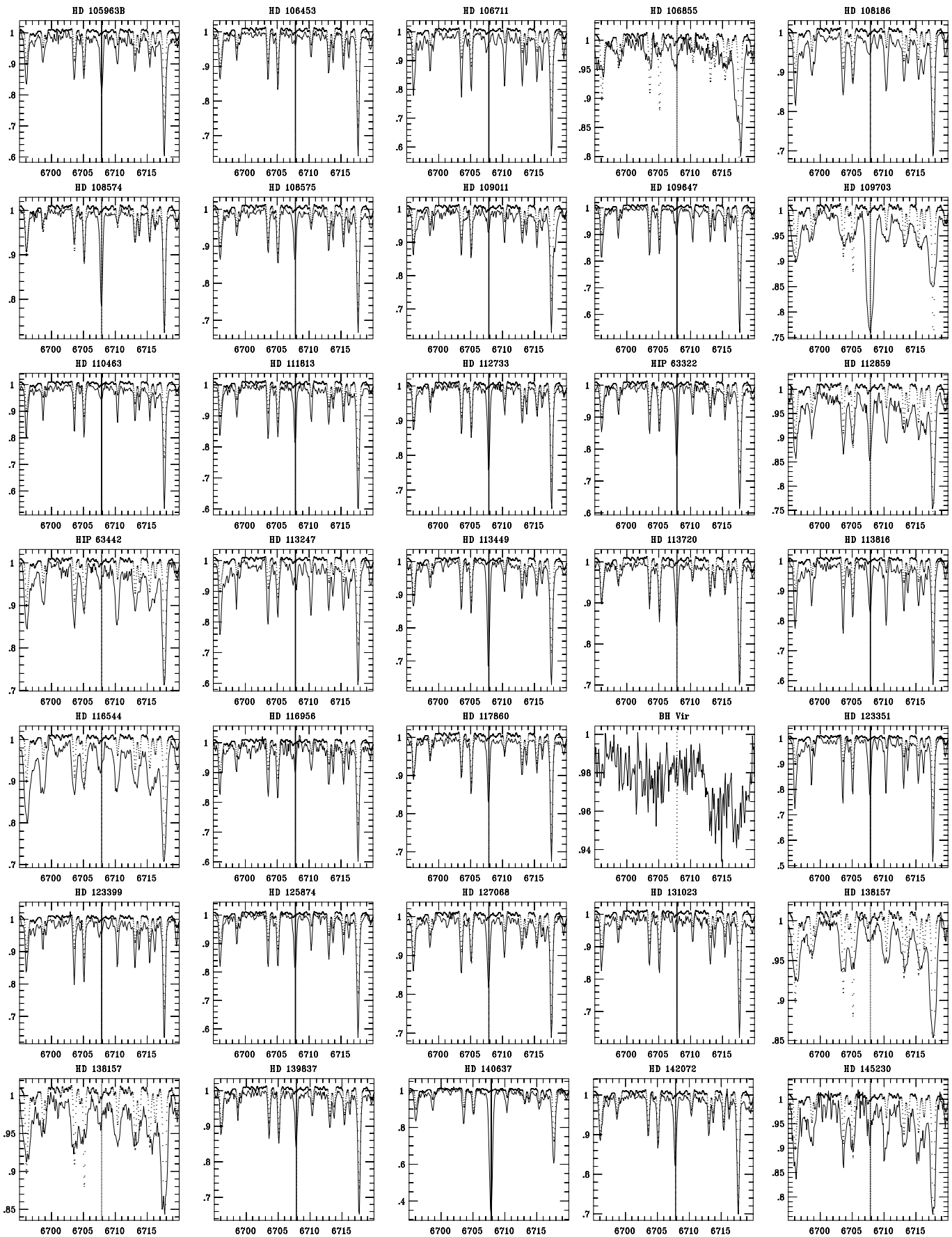

Fig. B3. continued

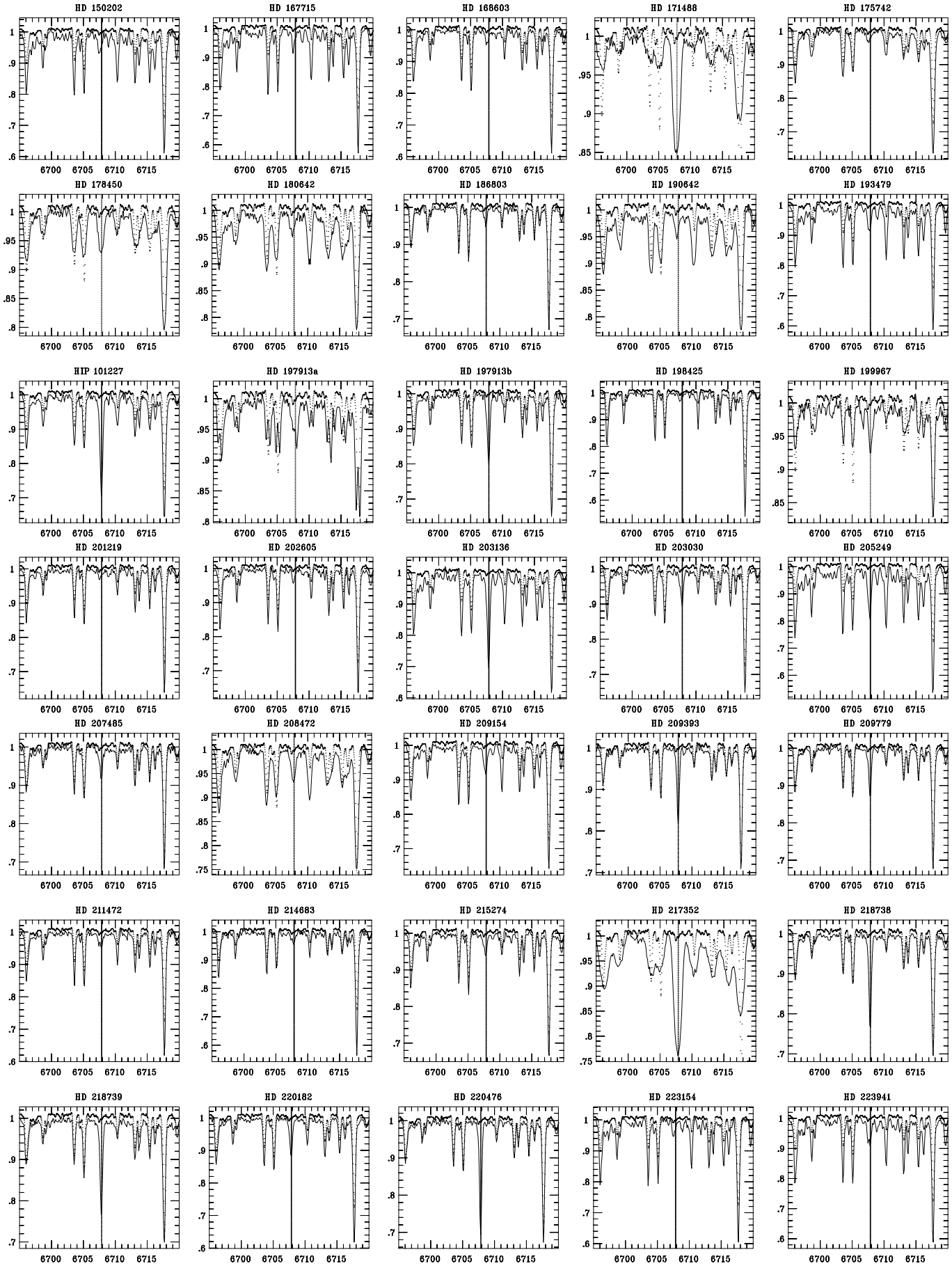

Fig. B3. continued

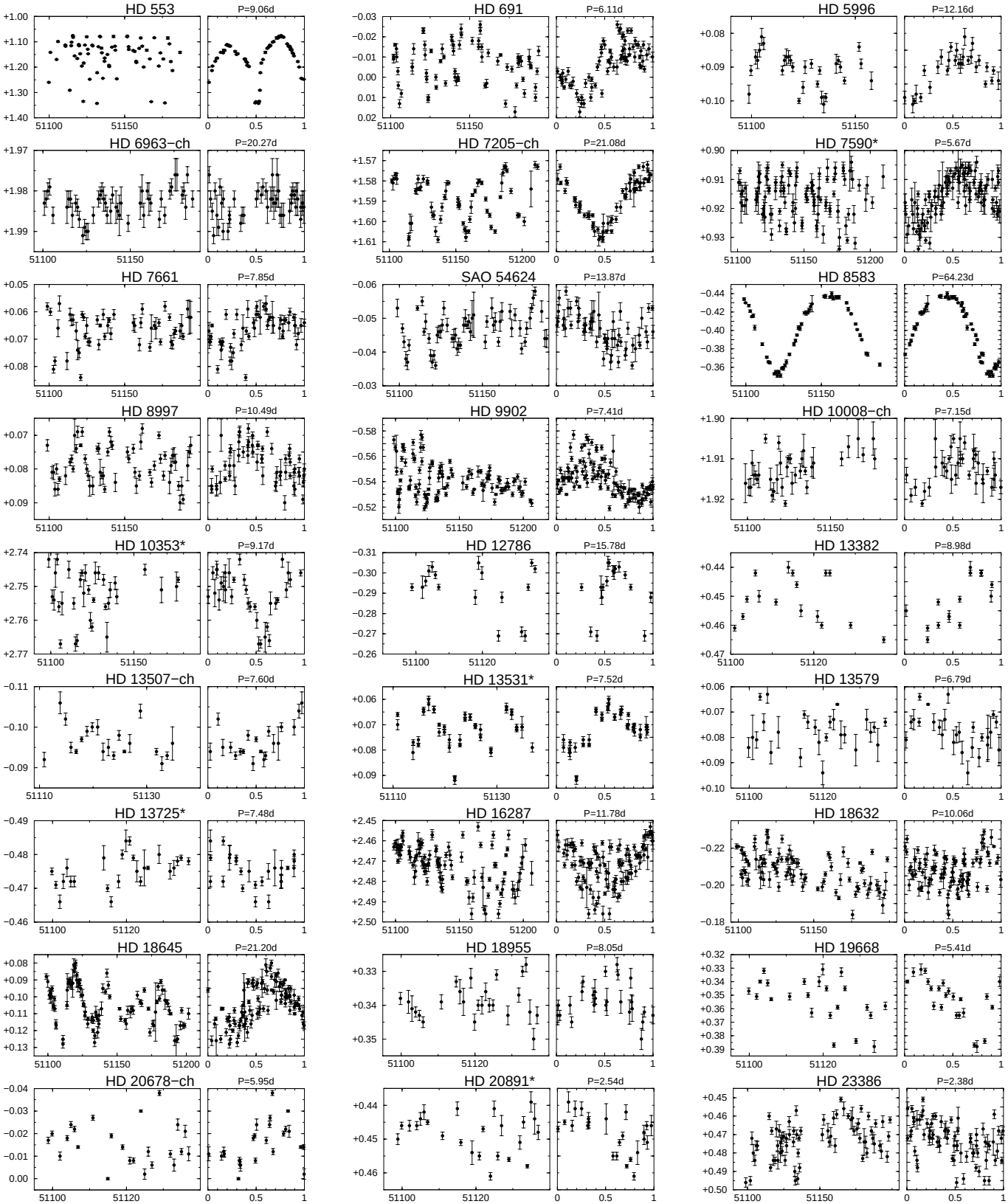

Fig. B4. Differential Strömgren-y light curves of stars with Ca II H and K emission. The HD number (or HIP number, or Variable Star designation, if no HD number exists) is identified on top of each plot. The left panel in each plot is the observations versus heliocentric Julian date. The right panel is the light curve phased with the best-fit photometric period from Table A3. Error bars for the observations indicate the variances from three individual readings between the variable and the comparison star

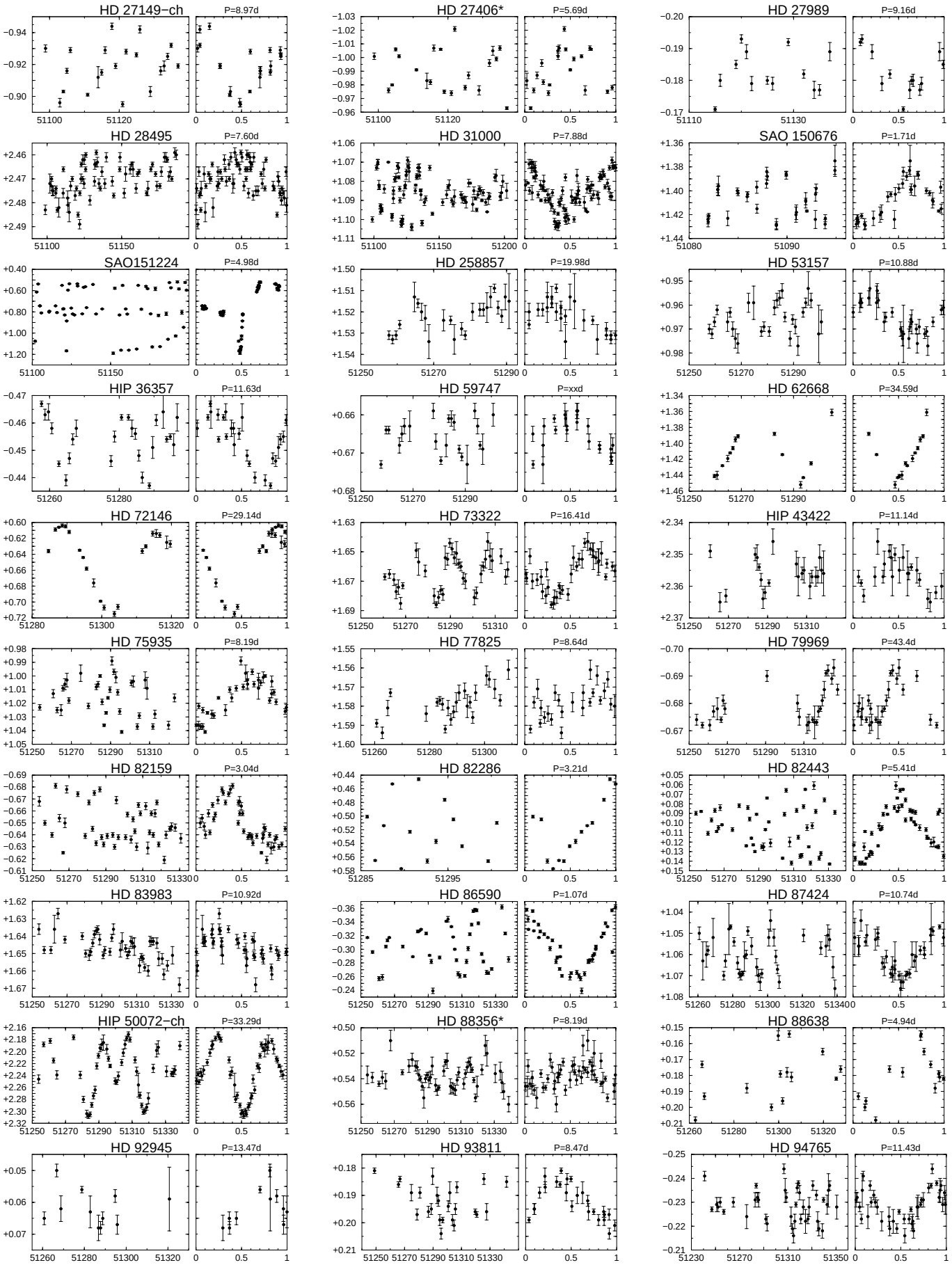

Fig. B4. continued

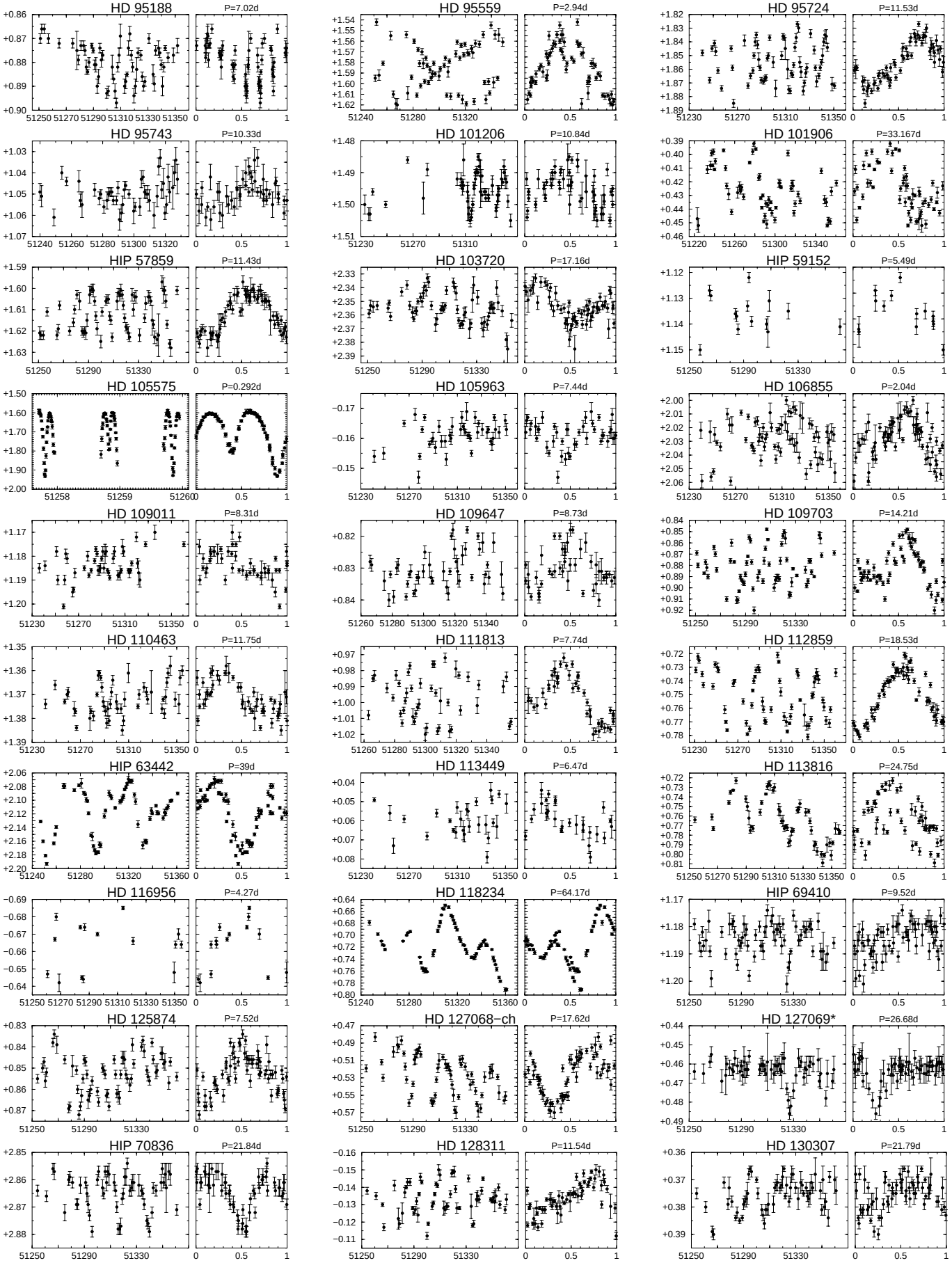

Fig. B4. continued

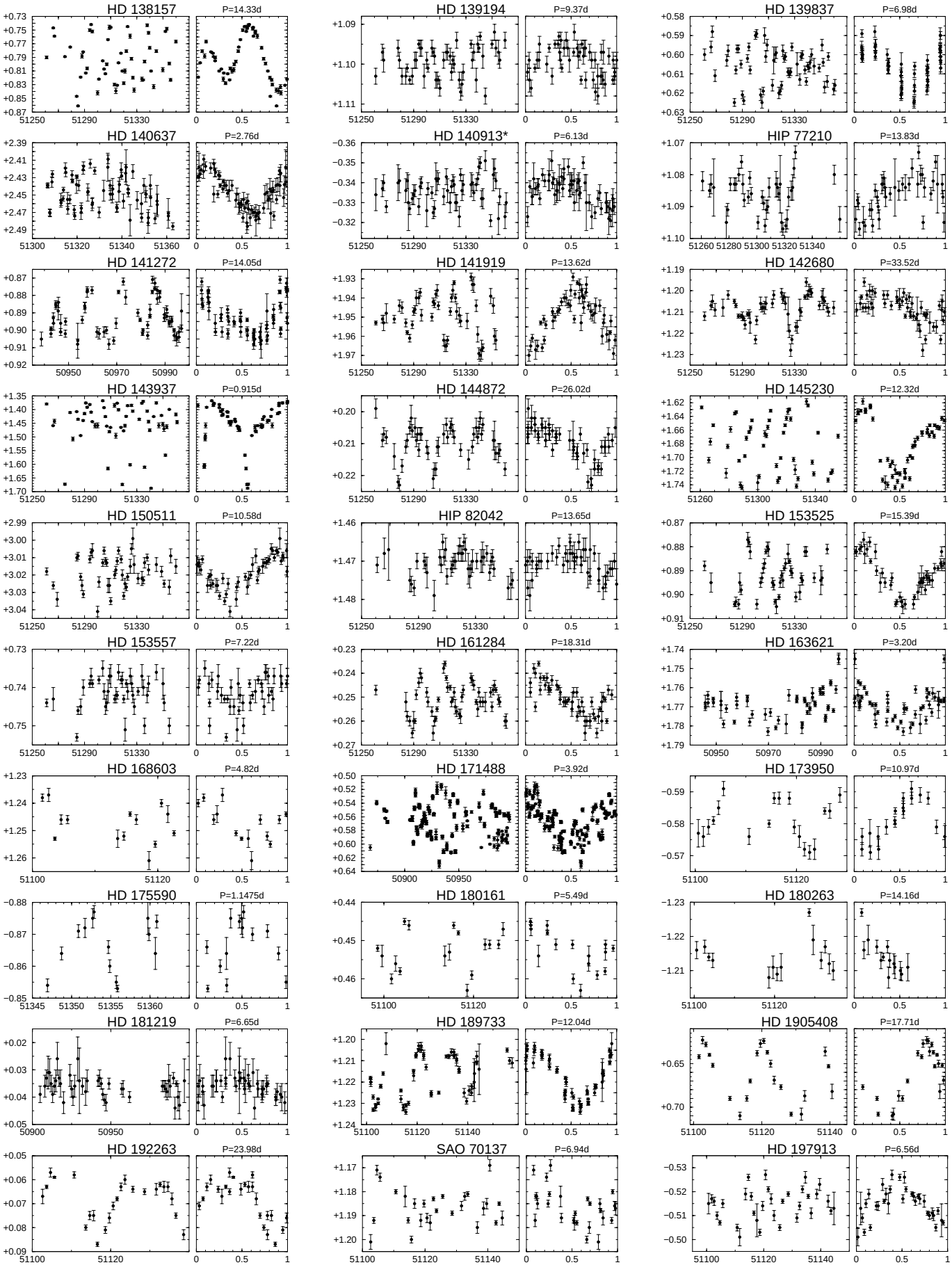

Fig. B4. continued

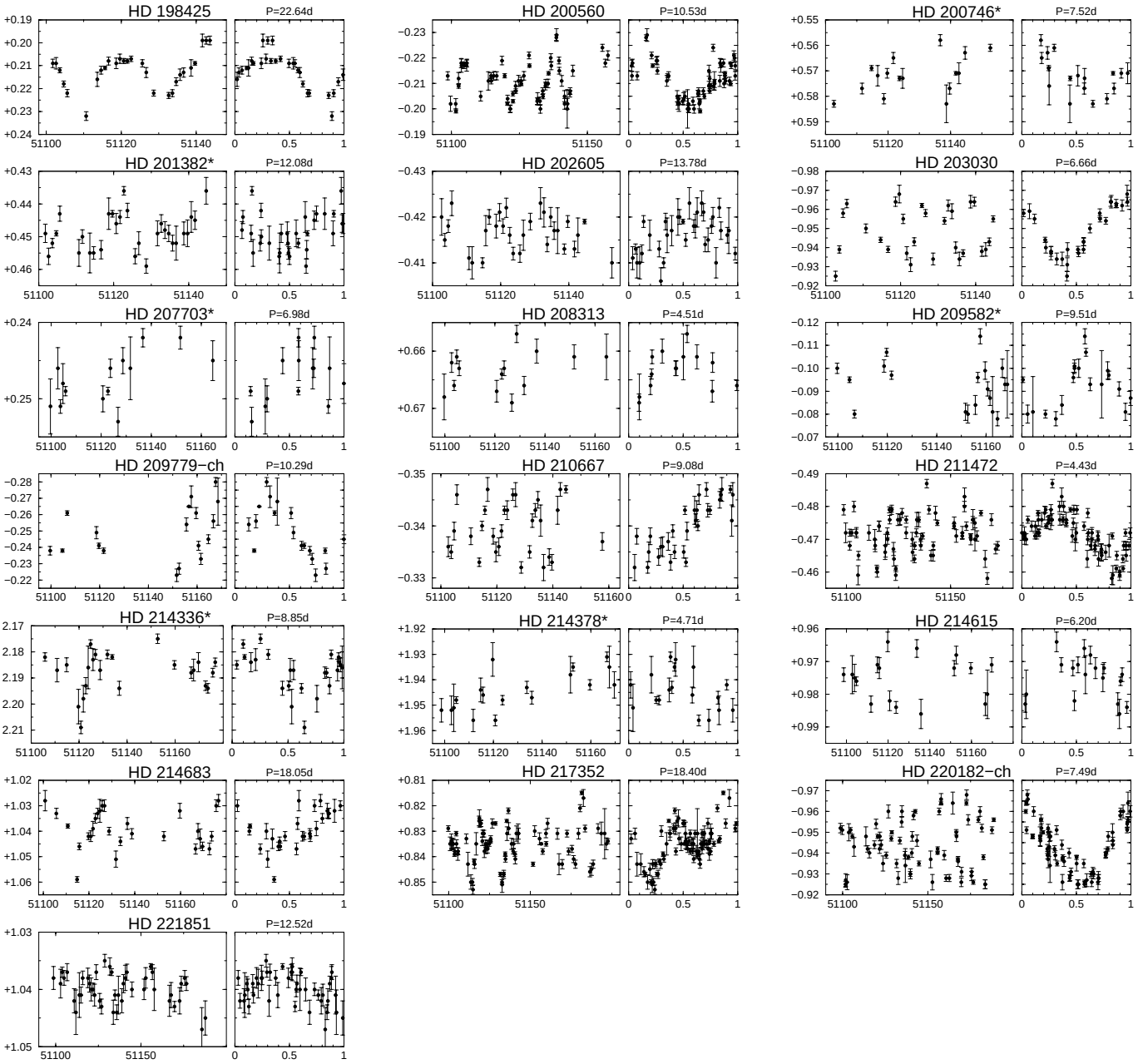

Fig. B4. continued

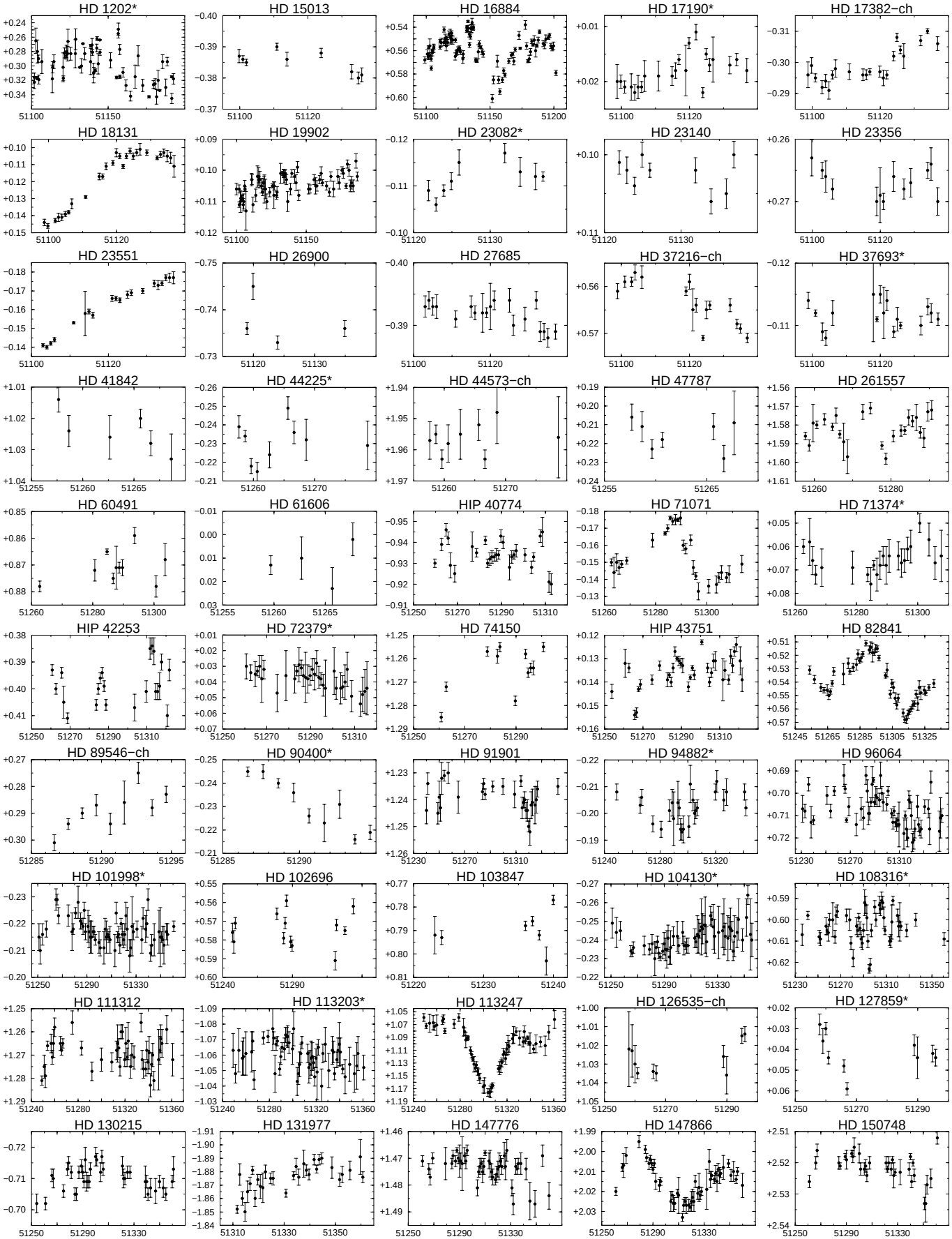

Fig. B5. Differential Strömgren-y light curves of stars without a period determination. Note that many of these stars are likely photometric variable but the time coverage was just too short to cover a full cycle. Otherwise as in Fig. B4

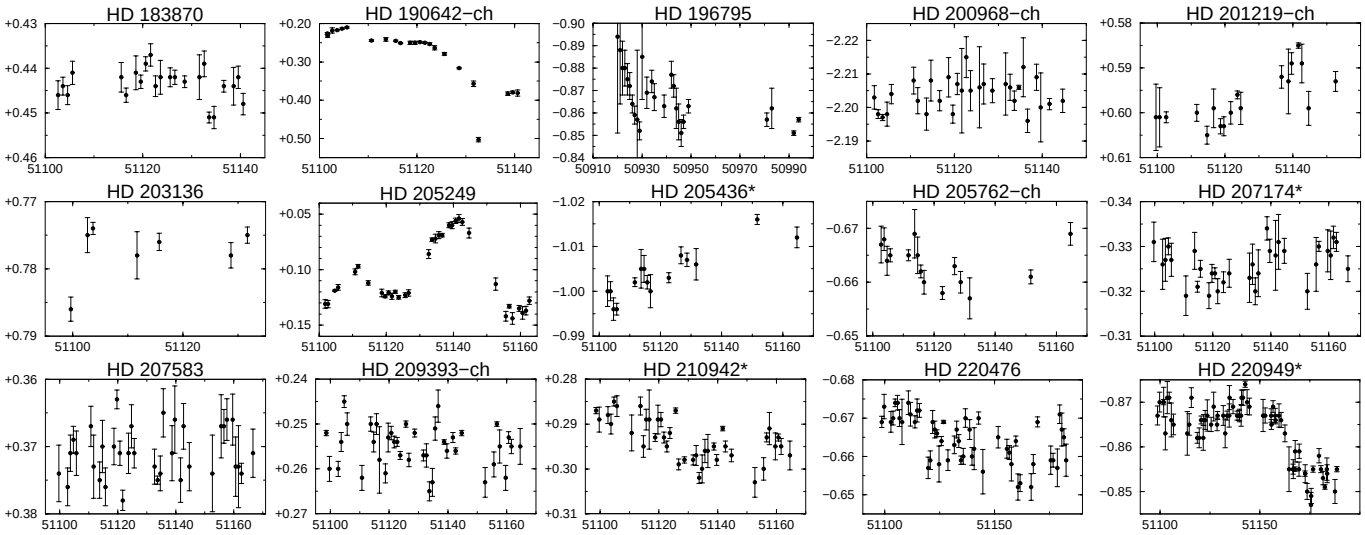

Fig. B5. continued